Functional redundancy and formin-independent localization of tropomyosin isoforms in Saccharomyces cerevisiae

Anubhav Dhar[a,c], Bagyashree VT[a,c], Sudipta Biswas[b], Jayanti Kumari[a], Amruta Sridhara[a], Jeevan Subodh B[a], Shashank Shekhar[b], Saravanan Palani[a*]

[a]Department of Biochemistry, Indian Institute of Science, Bengaluru, Karnataka 560012, India

[b]Departments of Physics, Cell Biology and Biochemistry, Emory University, Atlanta, GA, 30322, USA

[c]equal contribution

[*]Correspondence: spalani@iisc.ac.in

Abstract

Tropomyosin is an actin binding protein which protects actin filaments from cofilin-mediated disassembly. Distinct tropomyosin isoforms have long been hypothesized to differentially sort to subcellular actin networks and impart distinct functionalities. Nevertheless, a mechanistic understanding of the interplay between Tpm isoforms and their functional contributions to actin dynamics has been lacking. In this study, we present and charcaterize mNeonGreen-Tpm fusion proteins that exhibit good functionality in cells as a sole copy, surpassing limitations of existing probes and enabling real-time dynamic tracking of Tpm-actin filaments *in vivo*. Using these functional Tpm fusion proteins, we find that *S. cerevisiae* Tpm isoforms, Tpm1 and Tpm2, colocalize on actin cables and indiscriminately bind to actin filaments nucleated by either formin isoform- Bnr1 and Bni1 *in vivo*, in contrast to the long-held paradigm of Tpm-formin pairing. We show that cellular Tpm levels regulate endocytosis by affecting balance between linear and branched actin networks in yeast cells. Finally, we discover that Tpm2 can protect and organize functional actin cables in absence of Tpm1. Overall, our work supports a concentration-dependent and formin isoform independent model of Tpm isoform binding to F-actin and demonstrates for the first time, the functional redundancy of the paralog Tpm2 in actin cable maintenance in *S. cerevisiae.*

Introduction

Tropomyosins (Tpm) are a major class of actin-binding proteins present in fungi[1] and metazoans[2–4]. Tropomyosins are helical coiled-coil proteins that form head-to-tail dimers and co-polymerize with actin filaments[5–8]. Tpm was initially discovered as a component of muscle[9] where it regulates actomyosin contraction[10,11]. Later studies revealed that Tpm isoforms are also abundant in non-muscle cells[4,12–14] and even single-celled eukaryotic organisms like fungi[13,15,16]. The canonical role of non-muscle Tpm is to protect actin filaments from actin-severing proteins like cofilin[17–19] and thus regulate turnover of actin networks[20]. Tpms display a great diversity of isoforms across species with involvement in various cellular processes such as cell motility[21], cell division[13], organellar movement, secretory vesicle delivery, etc.[2–4,22]. Mammals have four tropomyosin genes which produce around 40 isoforms via alternate splicing[2,14,23]. Various studies have shown that Tpm isoforms sort extensively to distinct actin filament subpopulations and define diverse functionalities for these networks by controlling the interactions between F-actin and other actin-binding proteins such as myosin, cofilin, capping protein, etc.[2,4,24–29]. The molecular basis for Tpm isoform sorting remains an unresolved question with various mechanisms such as concentration dependence[30] or a formin-dependent targeting[31,32] having been observed. Structural analysis using cryoEM has now revealed that Tpm isoforms may exert differential functions via different modes of binding and controlling accessibility of ABPs like myosin and cofilin to F-actin[33,34]. How Tpm isoforms have been fine-tuned to perform distinct spatial sorting and functions during evolution remains an active area of research and their crosstalk during recruitment and maturation within the same actin structure is just beginning to be understood[21,35].

The eukaryotic model organism *Saccharomyces cerevisiae* has two tropomyosin isoforms encoded by two different genes- *tpm1* and *tpm2*[1,15,16]. Tpm1 (199 amino acids) is considered a duplicated paralog of Tpm2 (161 amino acids) with a 38 amino acid internal duplication[16]. Tpm1 is considered the major isoform and Δ*tpm1* cells display a near complete loss of actin cables and lethality at higher temperatures[13,28,29]. Δ*tpm2* cells on the other hand show no detectable changes in actin cable organization and cell growth[16,36]. Interestingly, deletion of both *tpm1* and *tpm2* is synthetic lethal[16]. Cells compromised in actin severing factors such as Δ*aip1* or Δ*srv2* mutants show partial restoration of cables in Δ*tpm1* cells which suggests that Tpm1 is majorly involved in protection of the actin filaments from severing proteins of the CCA (Cofilin-Coronin-Aip1) complex *in vivo*[37,38]. The minor isoform Tpm2 is expressed at ~5 fold lower levels and Tpm2 overexpression could not restore normal growth and actin cables in Δ*tpm1* cells in a previous study[16]. The *in vivo* functions of Tpm2 have remained unclear but studies have suggested a role for Tpm2 in negatively controlling retrograde actin cable flow (RACF) possibly via regulating actin filament binding of the type-II myosin Myo1, which is positive regulator of RACF[39,40]. Both Tpm1 and Tpm2 facilitate processive motion of the type-V myosin Myo2 on coated actin filaments *in vitro*[41], contributing to the anterograde flow of organelles

and cargo to the growing bud[22,42,43]. Thus, Tpm1 is believed to play a major role in maintaining the actin cytoskeleton in yeast while the functions of Tpm2 are believed to be majorly distinct from Tpm1[16]. While genetic studies have indicated a possible preference between Tpm isoforms and formin isoforms[36], whether Tpm1 and Tpm2 localize to distinct actin filaments/cables in *S. cerevisiae* has remained unaddressed mainly due to absence of functional Tpm fluorescent fusions and live-cell imaging data for Tpm1 and Tpm2. Recent work from our lab made it possible to visualize the live dynamics of Tpm across species using mNG-Tpm fusion proteins[44] for the first time and revealed their localization to actin cables and the actomyosin ring during the cell cycle[44]. However, their combined action and roles in actin cable stability *in vivo* is not understood.

In this study, we assess the functionality of mNeonGreen-Tpm fusion proteins and show that mNG-Tpm fusion proteins are functional and restore viability as sole copies in cells lacking native Tpm1 and Tpm2. We also engineer -AS- dipeptide containing mNG-^{AS}Tpm constructs to account for lack of N-terminal acetylation and improve functionality *in vivo*. Using mNG-^{AS}Tpm fusion proteins, we find that Tpm1 and Tpm2 indiscriminately associate with actin filaments made by either formin Bnr1 and Bni1, unlike the differential association of acetylated and unacetylated Cdc8 to distinct formin-nucleated filament populations shown in *S. pombe*[31,45]*.* We report a novel function of Tpm2 and show that Tpm2 can compensate for loss of Tpm1 upon increased expression *in vivo.* In contrast to the long-held view, we find that increased Tpm2 expression can restore full length actin cables and actin-cable dependent functions such as vesicle targeting to bud and maintenance of normal mitochondrial morphology suggesting that Tpm2 can independently organize a functional actin cable network in *S. cerevisiae* in the absence of Tpm1. Lastly, we also report the role of Tpm1 and Tpm2 in maintaining linear-to-branched actin network homeostasis in yeast, revealing an intriguing cascading effect of Tpm on actin dynamics at sites of endocytosis. Overall, our findings support a concentration-dependent and formin-independent localization of Tpm isoforms to actin cables and unveil the functional redundancy between Tpm isoforms in *S. cerevisiae.*

Results

mNG-Tpm fusion proteins are functionally-active tagged Tropomyosin fusion proteins

Visualization of tropomyosin in live cells has been a major challenge because fluorescently-tagged tropomyosin fusions are not completely functional and thus, need careful interpretation for accurate insights about Tpm localization and dynamics *in vivo*[46]. We have recently shown that mNeonGreen-Tpm (mNG-Tpm) fusion proteins clearly report localization of Tpm isoforms to actin structures *in vivo* in fungal and mammalian cells[44] **(Fig. S1A, S1B)** but their functionality compared to native Tpm remained unknown. To address if mNG-Tpm fusion proteins could compensate for loss of native Tpm in cells, we assessed complementation of cellular defects caused by deletion of *tpm1* gene by mNG-Tpm1 expressed under the native *tpm1* promoter. We found that mNG-Tpm1 expression could near completely restore normal growth **(Fig. S1C, S1D)** but only partially restore the length of actin cables

in Δ*tpm1* cells which exhibit slower growth and absence of actin cables **(Fig. S1G, 1C)**. The presence of shorter actin cables suggests partial functionality of mNG-Tpm1 fusion as compared to the native Tpm1 protein and that partial length cables are sufficient to majorly support normal growth via proper cargo targeting to the bud. One possible explanation for presence of shorter actin cables is the lack of N-terminal acetylation of mNG-Tpm by the Nat3-Mdm20 complex which is essential for normal Tpm-actin binding *in vivo*[47–49]. This could result in reduced binding affinities towards F-actin as compared to native Tpm. Thus, we constructed mNG-^{AS}Tpm, a modified mNG-Tpm fusion protein with an Ala-Ser dipeptide before the starting methionine of Tpm that has been routinely used to restore normal binding affinities by stabilizing the N-terminal alpha-helix in the absence of the N-terminal acetylation[25,36,50–52]. Live-cell imaging of cells expressing mNG-^{AS}Tpm fusion protein as an integrated single copy showed improved but clear signal enhancement of both mNG-^{AS}Tpm1 and mNG-^{AS}Tpm2 on actin cables and the actomyosin ring **(Fig. 1A, S1H, Supplementary Movie 1-2)**. mNG-^{AS}Tpm1 expression could completely rescue the growth defects **(Fig. S1C, S1D)** and restore full-length actin cables in Δ*tpm1* cells when expressed at similar levels as mNG-Tpm1 **(Fig. 1B, 1C)**. These results clearly indicate that mNG-^{AS}Tpm1 is a functional tagged tropomyosin with similar activity as native Tpm1. To test for functionality of tagged Tpm2, we expressed mNG-Tpm1, mNG-^{AS}Tpm1, mNG-Tpm2, mNG-^{AS}Tpm2 under their native promoters in Δ*tpm1*Δ*tpm2* cells containing a copy of Tpm1 in a *ura3*-centromeric plasmid. Shuffling of these strains to 5'FOA-containing media revealed that all mNG-Tpm fusions rescued synthetic lethality of Δ*tpm1*Δ*tpm2* cells when expressed from a high-copy plasmid (*pRS425*) **(Fig. S1E)** but only mNG-Tpm1 and mNG-^{AS}Tpm1 restored viability when expressed from single-copy integration plasmid (*pRS305*) **(Fig. S1F)**. This suggests that both mNG-Tpm1 and mNG-Tpm2 fusions are functional tagged Tpm fusions and Tpm1 tolerates the presence of the N-terminal tag better than Tpm2. Next, we tested whether actin cables restored by mNG-Tpm1 and mNG-^{AS}Tpm1 are functional and assessed mitochondrial morphology as a readout of function. We found that mitochondrial fragment number is restored to wildtype levels by expression of both mNG-Tpm1 and mNG-^{AS}Tpm1 in Δ*tpm1* cells which show hyper-fragmented mitochondria[53,54], suggesting again that full length cables are not necessary for restoring downstream actin cable-dependent functions. These data also suggest that Tpm mediated actin cable stability *in vivo* may be one of the factors determining actin cable length control with cell size in yeast[55,56] **(Fig. 1D, S1G)**.

Taken together, our results demonstrate that mNG-Tpm fusion proteins are functional, and acetylation-mimic improves their functionality in vivo, thus, expanding their applicability to probe a broad range of questions about Tpm isoform biology.

Tpm1 and Tpm2 indiscriminately bind to actin cables nucleated by both formin isoforms

Tpm isoforms are known to sort to distinct actin filament structures in space and time in various organisms[4,4,24,32,32,33,45,57–61] and the basis of this spatial sorting remains an enigmatic question[30,62]. N-terminal acetylated and unacetylated forms of the fission yeast Tpm, Cdc8, show a formin-dependent

spatial sorting to distinct actin cable networks[31,45]. Contrasting results from studies in mammalian cells support both formin-mediated[31,32] or relative concentration-dependent sorting mechanisms[30]. The presence of two Tpm isoforms maintained at distinct expression levels (Tpm1 expressed ~5-6 fold higher than Tpm2)[16,63] and previous observations showing that Δ*tpm1* exhibits distinct genetic interactions with either formin- Bnr1 and Bni1 indicates a possible crosstalk between Tpm and formin isoforms in *S. cerevisiae*[36]. Tpm1 also increased Bni1-mediated nucleation of actin filaments in an *in vitro* assay without having any effect on Bnr1-mediated nucleation in the same study[36]. However, whether these differences observed *in vitro* translate to measurable effects and possible formin-based spatial sorting of Tpm1 and Tpm2 *in vivo* remains unclear. To answer these questions, we investigated if Tpm1 and Tpm2 preferred actin cables nucleated by a specific formin isoform - Bnr1 or Bni1. Bnr1 and Bni1 localize to the bud neck and bud cortex respectively from G1 till onset of cytokinesis where they nucleate distinct sets of actin filaments[64–68]. Localization of both Tpm1 and Tpm2 on actin cables could be observed in both Δ*bnr1* and Δ*bni1* cells **(Fig. 2A, 2D)**, qualitatively suggesting that both Tpm1 and Tpm2 bind to actin cables nucleated by either formin - Bnr1 and Bni1 indiscriminately.

To assess for any minor biases in preference shown by Tpm1 and Tpm2 for formins Bnr1 and Bni1, we then performed an extensive quantitative analysis of actin cable organization visualized by phalloidin staining **(Fig. S2A, S2D)** and Tpm localization visualized by mNG-^{AS}Tpm1/2 fusion proteins in wildtype, Δ*bnr1,* and Δ*bni1* cells expressed under their native promoters from an extra integrated copy at the *leu2* locus **(Fig. 2A, 2D)**. However, mNG-^{AS}Tpm signal drastically weakened after fixation making it difficult to score properly for Tpm localization. Hence, we measured average actin and Tpm-bound actin cable length and number in these strains as a population average instead of simultaneous co-staining in single cells **(Fig. 2A, 2D, S2A, S2D)**. Our analysis revealed that actin cable numbers dropped significantly upon deletion of either formin Bnr1 and Bni1 suggesting a redundant role for both formins in actin cable nucleation **(Fig. S2C, S2F),** while actin cable lengths were longer in *Δbnr1* as compared to both wildtype and Δ*bni1* cells **(Fig. S2B, S2E)** which could be explained by the elongated cell shape observed in Δ*bnr1* cells **(Fig. S2A, S2D)***.* Both Tpm1- and Tpm2-bound cable length did not show a consistent signifiant change between wildtype*,* Δ*bnr1, and* Δ*bni1* cells **(Fig. 2B, 2E)**. The average number of Tpm1- and Tpm2-bound cables per cell were reduced in Δ*bnr1 and* Δ*bni1* cells as compared to *wildtype* **(Fig. 2C, 2F)** but the reduction was comcomitant with the reduction in actin cable numbers observed in Δ*bnr1 and* Δ*bni1* **(Fig. S2C, S2F)** and no major dependence on either formin was observed for both Tpm1 and Tpm2. The ratio of mNG-^{AS}Tpm1 and mNG-^{AS}Tpm2 fluorescence in the bud to the mother compartment increased in Δ*bnr1* cells and decreased in Δ*bni1* cells as compared to wildtype cells **(Fig. S2G)**, consistent with the fact that Bnr1 nucelates cables only in the mother compartment and all cables present in the bud compartment are nucleated by Bni1 **(Fig. S2A, S2D)**. This suggests that Tpm1 and Tpm2 do not show preference for binding to cables in either bud or mother compartment as shown recently for another actin cable-

binding protein, Abp140[69]. Since, mNG-^{AS}Tpm1 is functional when expressed under native Tpm1 promoter **(Fig. S1D, S1E)**, we also conducted our analysis in strains lacking endogenous Tpm1 and expressing only mNG-^{AS}Tpm1 to eliminate any effects of increased levels of functional Tpm1 protein. We found that mNG-^{AS}Tpm1 still localized to actin cables in wildtype, Δ*bnr1, and* Δ*bni1* cells **(Fig. S3A)**. Tpm-bound actin cable length and Tpm-bound actin cable number was decreased in Δ*bnr1* and Δ*bni1* cells as compared to wildtype **(Fig. S3B, S3C)**, which was again concomitant with the decrease in actin cable length and number **(Fig. S3D, S3E, S3F)**. Thus, our quantitative analysis also suggests that Tpm1 and Tpm2 binding to actin cables is unaffected by identity of the formin isoforms-Bnr1 and Bni1, implicating that they indiscriminately bind to both Bnr1- and Bni1-nucleated actin cables in *S. cerevisiae.*

Lastly, we assessed if Tpm1 and Tpm2 localize to the same set of actin cables *in vivo* by co-expressing ymScarleti-^{AS}Tpm1 and mNG-^{AS}Tpm2 fusion proteins. We observed that both ymScarleti-^{AS}Tpm1 and mNG-^{AS}Tpm2 localized to the same set of actin cables **(Fig. 2G)** in cells indicating that they may either co-polymerize on a single actin filament or are bound to different actin filaments bundled together into an actin cable.

Overall, our qualitative and quantitative analysis suggests that Tpm1 and Tpm2 indiscriminately bind to actin filaments nucleated by either formin, Bnr1 and Bni1, and do not exhibit spatial sorting to distinct actin cable networks in *S. cerevisiae*. Since, Tpm1 and Tpm2 have differential expression levels in cells, their relative local concentrations may be the major factor in determining their localization to actin filament networks in *S. cerevisiae* and governing their functions.

Tpm1 and Tpm2 localize to the fusion focus in a Bnr1-independent manner in mating yeast cells

Polarized actin assembly is required for growth of the pheromone-induced mating projection (shmoo) in yeast cells[70–72]. Similar to polarized bud growth, formin-made actin cables act as tracks for vesicles to be delivered to the tip of the mating projection where coordinated exo- and endo- cytosis ensure polarized growth, membrane turnover, and cell wall remodelling[73,74]. It has been shown that Δ*tpm1* cells require much higher pheromone concentrations for shmoo formation as compared to wildtype cells[75]. To assess whether both Tpm1 and Tpm2 localized to the actin cables in the mating projection, we mated wildtype *MAT-a* haploid yeast cells expressing either mNG-^{AS}Tpm1 or mNG-^{AS}Tpm2 with wildtype *MAT-*α yeast cells. Both mNG-^{AS}Tpm1 and mNG-^{AS}Tpm2 localized to the mating projection tip **(Fig. 3A, Supplementary movie 3-4)** and their level started gradually decreasing ~2-4 minutes before fusion of cells could be observed **(Fig. 3C)**. These results demonstrate that Tpm1 and Tpm2 localize to the mating fusion focus and suggest a role for them in stabilizing formin-based actin cables during yeast mating. Previous studies have shown that the pheromone induced shmoo formation is dependent only on the formin Bni1 which is recruited via Bil2 and requires Bud6 activity[71,76]. So, we performed another experiment where we mated Δ*bnr1* cells expressing either mNG-^{AS}Tpm1 or mNG-

184 ^{AS}Tpm2 with wildtype cells of opposite mating type. We observed that both mNG-^{AS}Tpm1 and mNG-
185 ^{AS}Tpm2 localized to the mating projection tip with similar kinetics in Δ*bnr1* cells similar to wildtype
186 cells **(Fig. 3B, 3D)**, suggesting that both Tpm1 and Tpm2 bind to Bni1-made actin filaments at the
187 mating projection during the pheromone response in *S. cerevisiae.* These observations suggest a
188 role for Tpm1 and Tpm2 in stabilization of Bni1-made actin cables during yeast mating and further
189 strengthen our conclusion that Tpm1 and Tpm2 indiscriminately bind to formin-made filaments
190 irrespective of the identity of the formin isoform in *S. cerevisiae*.
191
192 **Tpm1 and Tpm2 protect equally well from cofilin-mediated actin filament severing**
193 Tpm1 and Tpm2 isoforms are believed to play both shared and distinct roles in *S. cerevisiae*[16,39]*.* The
194 major isoform Tpm is expressed 5-6 fold higher than Tpm2 and its absence leads to a near complete
195 loss of actin cables[15,36,75] **(Fig. S4B)**. A previous study reported that overexpression of Tpm2 could
196 not restore actin cables in a Δ*tpm1* strain suggesting that Tpm2 and Tpm1 may have distinct
197 functions[16]. We were intrigued by this observation as Tpm1 and Tpm2 have identical subcellular
198 localization and dynamics as revealed by live-cell imaging of mNG-Tpm fusion proteins **(Fig. 1A, 2G)**.
199 Thus, we decided to revisit Tpm2 functionality and determine its subcellular roles in maintaining the
200 actin cytoskeleton. Firstly, to test whether Tpm1 and Tpm2 impart similar protection against cofilin-
201 mediated severing, we performed an in-vitro TIRF imaging[77,78] with purified yeast tropomyosins
202 (Tpm1, Tpm2), human Tpm1.7[79] (positive control) and budding yeast Cofilin (Cof1) **(Fig. 4A)**. We
203 found that Tpm1.7, Tpm1 and Tpm2 coated-actin filaments displayed significantly lower severing
204 events per unit time and length **(Fig. 4B)** and resulted in higher filament lengths after 2 min of cofilin
205 addition as compared to uncoated control filaments **(Fig. 4C)**. These observations suggest that Tpm1
206 and Tpm2 display similar biochemical activities of actin filament protection from severing action of
207 cofilin, and hint towards an potential protective role of Tpm2 in cells.
208
209 **Tpm2 overexpression can compensate for loss of Tpm1 function *in vivo***
210 To coroborate our in-vitro findings and test whether Tpm2 could complement growth defects caused
211 by loss of Tpm1, we overexpressed Tpm2 in a Δ*tpm1* strain using a high-copy number plasmid and
212 surprisingly, found that Tpm2 overexpression could restore growth rates similar to wildtype levels in
213 Δ*tpm1* cells **(Fig. S4A)**. This intriguing finding led us to investigate whether Tpm2 overexpression
214 could also restore actin cables in Δ*tpm1* cells. Interestingly, we observed that Tpm2 overexpression
215 could rescue actin cables similar in length and number to wildtype in ~80% of Δ*tpm1* cells **(Fig. S4B,**
216 **S4C)**. We confirmed Tpm2 overexpression using RT-qPCR data which revealed a ~19 fold higher
217 Tpm2 mRNA abundance after expression through high-copy number plasmid (*pRS425-*^{pTpm2}*TPM2*)
218 as compared to Tpm2 mRNA levels in wildtype and Δ*tpm1* cells **(Fig. S4D)**. This data clearly suggests
219 that in contrary to previous understanding, elevated levels of Tpm2 can organize polarized actin
220 cables in the absence of Tpm1, potentially by protecting actin cables from the severing action of

221 cofilin. This represents a previously unrecognized activity for Tpm2 and raises further interesting
222 questions about the shared and distinct roles of Tpm isoforms in *S. cerevisiae.*
223

224 **Mild increase in Tpm2 expression can restore actin cable organization in Δ*tpm1* cells**

225 We assessed if increasing Tpm2 protein levels via low-copy plasmid expression under native Tpm1
226 and Tpm2 promoters (^{pTpm1}*TPM1* and ^{pTpm2}*TPM2*) could rescue defects of Δ*tpm1* cells. We tested their
227 ability to rescue growth of Δ*tpm1* cells and found that both ^{pTpm2}*TPM2* and ^{pTpm1}*TPM2* constructs
228 restored wildtype growth levels in Δ*tpm1* cells **(Fig. S4F)**. Expression of ^{ptpm2}Tpm1 and ^{pTpm1}*TPM1*
229 (positive control) also restored normal growth levels in Δ*tpm1* cells **(Fig. S4F)**. F-actin staining with
230 Alexa488-phalloidin showed rescue of actin cables by all Tpm2 and Tpm1 expression constructs in
231 ~90% Δ*tpm1* cells **(Fig. 5A, 5B)** to similar length as the wildtype **(Fig. 5C)**. To determine the amount
232 of Tpm2 mRNA after expression through low-copy plasmids, we performed RT-qPCR and found that
233 Tpm2 mRNA levels showed ~2 fold average increase when expressed under the pTpm1 promoter
234 and did not show any detectable change from wildtype levels when expressed under its native *ptpm2*
235 promoter **(Fig. S4E)**. Wildtype and Δ*tpm1* cells had similar Tpm2 mRNA levels suggesting Tpm2
236 expression is not sensitive to loss of Tpm1 **(Fig. S4F)**. In the absence of specific antibodies against
237 Tpm1 and Tpm2, we used the functionality of mNG-^{AS}Tpm fusion proteins to rescue phenotype in
238 Δ*tpm1* cells and ascertain that increased protein levels of Tpm2 are reponsible for the rescue. High-
239 copy plasmid (*pRS425*) expression of both mNG-^{AS}Tpm1 and mNG-^{AS}Tpm2 under their native pro-
240 moters rescued the severe growth defects of Δ*tpm1* cells at 37°C but only mNG-^{AS}Tpm1 and not
241 mNG-^{AS}Tpm2 rescued the defect when expressed from an integrated plasmid copy (*pRS305*) under
242 their native promoters **(Fig.S5A)**. Quantification of mean mNG signal intensity per cell revealed that
243 the highest expression was observed *in pRS425-*^{pTpm1}*mNG-*^{AS}*Tpm1* followed by *pRS425-*^{pTpm2}*mNG-*
244 ^{AS}*Tpm2*, *pRS305-*^{pTpm1}*mNG-*^{AS}*Tpm1* and pRS305-^{pTpm2}mNG-^{AS}Tpm2 **(Fig.S5B, S5C)**, consistent with
245 our earlier observation that mNG-Tpm2 fusion is functional at higher expression levels as compared
246 to native untagged Tpm2 **(Fig.S1E, S1F)**. We also performed western blotting with anti-mNG antibody
247 to detect protein levels **(Fig. S5D)** and found that *pRS425-*^{pTpm1}*mNG-*^{AS}*Tpm1* had the highest expres-
248 sion levels and *pRS425-*^{pTpm2}*mNG-*^{AS}*Tpm2* and *pRS305-*^{pTpm1}*mNG-*^{AS}*Tpm1* only expressed to ~20%
249 and ~10% of that level **(Fig. S5E).** Protein levels were not detectable in *pRS305-*^{pTpm2}*mNG-*^{AS}*Tpm2*
250 containing Δ*tpm1* cells **(Fig. S5D)** and in conjunction with our mean intensity analysis **(Fig. S5B, S5C)**
251 explain the lack of rescue observed in Δ*tpm1* cells containing *pRS305-*^{pTpm2}*mNG-*^{AS}*Tpm2*. Taken to-
252 gether, these data clearly suggest that it is the increase in mNG-^{AS}Tpm2 protein levels that lead to
253 rescue of observed phenotype in Δ*tpm1* cells.

254 Next, to test whether actin cable sensitivity is affected in cells lacking Tpm2, we assessed the
255 presence of actin cables after treatment with the actin monomer sequestering drug, Latrunculin B
256 (LatB) **(Fig. 5D)**. We found that Δ*tpm2* cells are significantly more sensitive to the depolymerizing

effect of LatB than wildtype cells **(Fig. 5D, 5E)**, suggesting that Tpm2 does play previously unrecognized detectable roles in actin cable stability in conditions of stress and contributes to robustness of the actin cable network.

Together, these results show that even minor increases in Tpm2 expression can restore normal actin cable organization in Δ*tpm1* cells suggesting that Tpm2 protein is present at limiting levels but retains the function of actin cable protection from severing factors like cofilin *in vivo* and *in vitro*. Tpm2 can, therefore, act as a safeguard mechanism for cells to protect against defects in Tpm1, providing functional redundancy and robustness against cellular stressors for actin cable maintenance in *S. cerevisiae.*

Tpm2 can solely organize a functional actin cable network in *S. cerevisiae*

Actin cables in *S. cerevisiae* are required for functions such as anterograde transport of vesicles and organelles[22,36,41,64,65,75], maintenance of mitochondrial inheritance and morphology[53,54,80,81], and clearance of protein aggregates from the bud[82,83] while retaining damaged mitochondria in the mother via retrograde actin cable flow (RACF)[40,84]. We asked whether Tpm2 organized actin cables could perform all these functions and if Tpm1-organized and Tpm2- organized actin cable networks had functional differences. We systematically analyzed these functional readouts using fluorescent reporters in wildtype, Δ*tpm1*, and Δ*tpm1* cells expressing Tpm2 in low-copy number and high-copy number plasmids. We used exogenous expressed ymScarleti-Sec4[36] integrated into the *ura3/leu2* locus to assess vesicle targeting to the bud via Myo2-dependent transport on actin cables[22] **(Fig. 6A, S6A)**. The ratio of bud-to-mother Sec4 fluorescence was calculated for all strains and the results showed that vesicle targeting to the bud was restored to levels similar to wildtype cells by expression of both ^{pTpm2}*TPM2* and ^{pTpm1}*TPM2* constructs **(Fig. 6C, S6C)**. Tpm1 expression also rescued vesicle targeting as a positive control under pTpm1 and pTpm2 promoters **(6A, 6C, S6C)**. These results suggest that both Tpm2 and Tpm1 can individually facilitate normal anterograde flow of cargo and vesicles to the growing bud via facilitation of Myo2 processivity on actin cables, in agreement with previous *in vitro* experiments where both Tpm1 and Tpm2 increased processivity of the type-V myosin, Myo2, on coated actin filaments[41].

Next, we assessed whether the hyper-fragmented mitochondrial morphology, a characteristic of Δ*tpm1* cells[53,54], could be restored by exogenous expression of Tpm2. For visualization of mitochondrial morphology, we used Su9-mNeonGreen[85] (subunit 9 of the F1-F0 ATPase fused to mNeonGreen) construct integrated at the *leu2/ura3* locus and quantified average mitochondrial fragment number per cell **(Fig. 6B, S6B)**. Δ*tpm1* cells showed increased mean mitochondrial fragment number as compared to wildtype while expression of Tpm2 or Tpm1 under native promoters in low copy or high copy plasmids restored the average mitochondrial fragment number to wildtype levels **(Fig. 6D, S6D)**. These results suggest that Tpm2-bound actin cables can interact and crosstalk normally with mitochondria to maintain its normal morphology. The underlying mechanisms of how actin cables

control mitochondrial morphology in budding yeast remain largely unknown and future studies are required to understand this enigmatic phenomenon.

Tpm2 has been previously implicated in negative regulation of retrograde actin cable flow (RACF) rates, possibly via its inhibitory effect on binding of the type-II myosin (Myo1) to actin filaments[39,40]. We independently replicated this experiment using LifeAct-eGFP[69,86] as an actin cable marker and corroborated that RACF rates are increased in the absence of Tpm2 and exogenous expression of Tpm2 and not Tpm1 in Δ*tpm2* cells restores RACF rates to wildtype levels **(Fig. S6E, S6F)**. RACF rates were similar to wildtype in Δ*tpm1* cells in which Tpm2 was expressed to restore actin cable suggesting again that loss of Tpm1 did not affect RACF rates in cells **(Fig. S6F)**. These observations suggest that Tpm2 has gained distinct regulatory function from Tpm1 in negatively regulating RACF while retaining its actin protective activity.

Global Tropomyosin levels are important for proper function and homeostasis between linear and branched actin in *S. cerevisiae*

Homeostasis between linear and actin networks in cells is maintained by various actin-binding proteins that coordinate and compete to generate actin filament network diversity in cells[87–91]. In yeast, formin proteins nucleate and maintain linear actin filaments which bundle and form cables[64,65] while Arp2/3 complex generates branched actin filaments which form a dense actin network at sites of endocytosis called actin patches[92,93]. Actin cables and patches interplay with each other while competing for the available cytoplasmic pool of actin monomers[88,90,94,95]. Tpm1 and Tpm2 localize to actin cables **(Fig. 1A)** and are majorly excluded from actin patches due to the activity of fimbrin (Sac6) which majorly localizes to actin patches[52,87]. We have previously shown that Tpm1 and Tpm2 localize to actin patches in Δ*sac6* cells[44] and a recent study observed similar targeting of Tpm to actin patches in the absence of Capping protein (Cap1/2 heterodimer) suggesting a tight regulation of protein composition between these two networks[89]. Tpm loss or overexpression has been shown to opposingly affect total number of actin patches[90]. We asked whether loss of actin cables observed in Δ*tpm1* cells could lead to effects on actin patch-mediated endocytosis. We used LifeAct-eGFP as a marker for actin patches **(Fig. 6E)** and observed that actin patch lifetime was significantly increased in Δ*tpm1* cells (~15 sec) as compared to wildtype and Δ*tpm2* cells (~10 sec) **(Fig. 6E, 6F)**. The increased patch lifetime was restored to wildtype levels upon exogenous expression of either Tpm1 or Tpm2 from a low-copy plasmid **(Fig. 6E, 6F)**, suggesting that the observed increase is caused due to the global decrease in Tpm levels and loss of actin cables, and not specifically due to loss of Tpm1. We next tested whether the loss of actin cables observed in Δ*tpm1* cells lead to increased accumulation of actin at the actin patches and found that mean LifeAct-eGFP intensity at actin patches was higher in Δ*tpm1* cells as compared to wildtype and Δ*tpm2* cells **(Fig. 6G)**. The mean intensity was restored to wildtype levels upon exogenous expression of Tpm1 and Tpm2 in Δ*tpm1* cells **(Fig. 6G)**, suggesting that reduction in global Tpm levels leads to dysregulation of actin cables, increased actin

accumulation at the actin patches, eventually leading to abnormal endocytosis dynamics. These results highlight the isoform independent importance of Tpm in maintaining normal balance and homeostasis between actin networks in a common cytoplasmic volume in *S. cerevisiae* and opens avenues for future study of actin network crosstalk via effects of actin-binding protein in yeast and other eukaryotes.

Overall, our results suggest that Tpm2 can independently organize a functional actin cytoskeleton in *S. cerevisiae*. Our work highlights a previously unappreciated function of Tpm2 and demonstrates functional redundancy between Tpm isoforms despite evolutionary divergence and evolution of distinct functions such as RACF regulation. This functional redundancy may benefit cells under stress conditions and contribute to robust cell survival and viability.

Discussion

Making Functional Tropomyosin fusion proteins

In this study, we characterize and present functional fluorescently tagged-tropomyosin fusion proteins which make it possible to probe tropomyosin isoform localization, functions, and competition with other actin-binding proteins in live cells. Building on our previous work[44], we have shown that mNG-Tpm1 and mNG-Tpm2 are functional and can restore viability of Δ*tpm1*Δ*tpm2* cells which display synthetic lethality **(Fig. S1E)**. To our knowledge, this represents the first demonstration and characterization of tagged tropomyosin proteins which clearly report localization while near completely restoring growth and actin organization in cells lacking native Tpms **(Fig. 1A-D)**. Previous work in *S. pombe* had also identified N-terminus of *S. pombe* Tpm (Cdc8) as being favorable for tagging while the C-terminal fusion rendered the protein completely non-functional[46]. A key difference in our study is the presence of a 40-amino acid linker between the fluorescent tag and the Tpm protein[44], which seems to enhance functionality and allow proper head-to-tail contacts between Tpm dimers, as evident by the clear localization observed on actin cables which is not seen in case of direct N-terminal tagging of Tpm[96]. N-terminal tagging also has its caveats as it blocks N-terminal acetylation of Tpm which is essential for normal Tpm binding to F-actin in cells[47,48] and also for regulation of other actin-binding proteins such as myosin-II and myosin-V[24,45]. To overcome this limitation, we generated mNG-^{AS}Tpm fusion proteins which contain an Alanine-Serine (-AS-) dipeptide to mimic the effect of N-terminal acetylation. The use of -AS- dipeptide is routinely used to purify Tpm proteins from *E. coli* as it restores normal binding affinity[50] and its addition to the N-terminus of Tpm in the mNG-Tpm fusion improved their functionality by restoring normal length of actin cables in our experiments **(Fig. 1B, 1C)**. The observed effect may be due to increased binding affinity of -AS- containing Tpm for F-actin in cells as compared to unacetylated tagged Tpm and also suggests a role for Tpm activity in cell size dependent scaling of actin cables in yeast. Previous work suggested that acetylation decreases the destabilizing effect of the positive charge of the N-terminus on the coiled-coil ‘a’ position where a hydrophobic residue normally resides[50]. A later study proposed that the -AS- dipeptide ensures that

368 the Met1 stays in an alpha-helical structure by introducing stabilizing hydrogen bonds between the
369 Ser and Met residues[97]. Thus, -AS- dipeptide addition likely does not mimic N-terminal acetylation
370 structurally but acts via maintaining N-terminus stability. Future work is required to understand in
371 detail the effects of the linker and -AS- dipeptide on Tpm biochemical activity and effect on interactions
372 with other actin-binding proteins (ABPs).
373
374 **Spatial sorting of Tpm isoforms**
375 The molecular basis of Tpm isoform sorting has remained an unresolved enigma in the field. Various
376 studies over the years have implicated different mechanisms for spatial sorting of Tpm isoforms
377 across different model systems. While *S. pombe* Tpm (Cdc8) exhibits sorting based on preference
378 between N-terminal acetylation status and formin isoform[45], mammalian Tpms have been proposed
379 to sort through either formin-based nucleation[32] or relative concentration dependent mechanisms[30].
380 However, N-terminal acetylation did not bias localization of Cdc8 to filaments made by a particular *S.*
381 *pombe* formin isoform in a minimal in-vitro reconstituted set-up[98], in contrast to the earlier in vivo
382 observations[45], suggesting that interaction of the distinct Cdc8 forms (unacetylated vs acetylated) with
383 distinct formins may not be enough for the spatial sorting observed and may require additional cellular
384 factors. In this study, we utilized our functional mNG-Tpm constructs to address this long-standing
385 question of Tpm isoform sorting in the model *S. cerevisiae* and find a formin-independent mode of
386 binding of Tpm isoforms to actin cables, in contrast to the formin-dependent modes observed in *S.*
387 *pombe*[31]. We also performed first-ever dual-color imaging of Tpm1 and Tpm2 simultaneously in live
388 cells which highlights the multiplexing possibilities of our tagging strategy to study Tpm isoform diver-
389 sity **(Fig. 2G)**. Strikingly, while *tpm1* shows distinct genetic interactions with formins Bnr1 and Bni1[36],
390 it did not show any preference for filaments made by any one of these isoforms in our study. This
391 seemingly contrasting observations could be explained by the observations from *Shin et. al., 2018*[99],
392 where difference in activities of Bnr1 and Bni1 in the presence of limiting levels of Tpm2 inside cells
393 could explain why loss of Bnr1 or Bni1 in Δ*tpm1* cells has opposite effects on cell growth and fitness.
394 Development of probes enabling measurement of formin activity in cells could help confirm this
395 hypothesis in the future. While it is possible that N-terminal tagging may influence formin-based Tpm
396 isoform sorting, C-terminally tagged constructs cannot currently be used to address this question due
397 to their non-functional nature. Thus, there is still scope for developments and improved strategies for
398 Tpm visualization to revisit these interesting questions. Overall, our data suggests distinct evolution-
399 ary adaptations and strategies for Tpm isoform sorting across species, which may be contingent on
400 species-specific needs and adaptations.
401
402 **Shared and Distinct functions of Tpm1 and Tpm2**
403 Our work also addresses the question of functional overlap and divergence of Tpm isoforms where
404 we report a previously unknown role of the “minor” isoform Tpm2 in actin cable protection suggesting

405 that Tpm2 has retained its actin protective function despite evolutionary divergence and gain of dis-
406 tinct regulatory activity in controlling retrograde actin cable flow as compared to Tpm1[39]. We find that
407 Tpm1 and Tpm2 protect equally well from cofilin *in vitro* **(Fig. 4D-F)**, suggesting that their binding sites
408 on F-actin may overlap with cofilin-binding site. However, their distinct regulation of Retrograde Actin
409 cable flow (RACF) which is controlled by myosin-II (Myo1) suggests distinct effects on myosin-II bind-
410 ing possibly through different overlap with myosin-II binding site on the actin filament[39]. Structural
411 data about their binding will reveal more insights into these possibilities. A possible reason why the
412 earlier study could not complement Δ*tpm1* cells with Tpm2 is the use of galactose-induction based
413 overexpression from a high-copy plasmid which would result in abnormally high levels of Tpm2 in
414 cells, causing toxicity and cell death[16]. From our results, it's clear that Tpm2 is present at limiting
415 levels and a mild increase in expression restores normal growth and actin cytoskeleton in Δ*tpm1* cells
416 **(Fig. 4A-C)**. The reason to keep such low levels might be to maintain Tpm2 specific function in RACF-
417 mediated asymmetric inheritance of damaged organelles and protein aggregates between mother
418 and bud[39,40,82,84], while also acting as a latent reservoir for actin cable maintenance in stressed
419 conditions. Consistent with this, we found cells lacking Tpm2 show decreased cable stability in
420 presence of the actin depolymerizing drug LatB **(Fig. 4G, 4H)**. Our data suggests that such functional
421 redundancy among diverged Tpm isoforms may confer robustness to actin-dependent processes and
422 increase chances of cell survival under certain stressed conditions. In the future, it remains to be
423 understood whether structural differences in F-actin binding modes[34] or other factors such as post-
424 translational modifications[25,48] in conjunction with expression levels and spatio-temporal regulation,
425 etc. contribute to the shared and distinct roles of closely related Tpm isoforms in *S. cerevisiae* and
426 other eukaryotes.
427
428 **Tropomyosin levels control global actin regulation and cross-talk of actin networks**
429 Actin monomeric pool in the cell is used to maintain diverse actin filament network types that differ in
430 geometry, composition of actin-binding proteins (ABPs), turnover and thus, their function[88]. Tropomy-
431 osin majorly binds to linear actin filaments nucleated by formin proteins and prevents branching of
432 linear actin filaments by inhibiting Arp2/3 complex-mediated branch nucleation on existing fila-
433 ments[88,98,99]. Linear actin cables and branched actin patches are the two major actin networks in yeast
434 with Tpm majorly localizing to the cables. Our data suggest that global decrease in Tpm levels not
435 only cause a loss of actin cables but also affect actin accumulation and dynamics at actin patches
436 which are sites of endocytosis **(Fig. 5E-G)**. This demonstrates that Tpm1 and Tpm2 levels are im-
437 portant for global actin network homeostasis and suggests that dysregulation of actin cables caused
438 by decreased Tpm levels trigger dysregulation of other actin networks which may contribute to cellular
439 defects observed in Δ*tpm1* cells. It remains to be addressed whether these effects are entirely due to
440 increased actin accumulation or also accompany changes in ABP composition of the branched actin
441 network. Future work with emphasis on network composition is required to delineate exact molecular

basis of such effects in cells with loss of normal actin network homeostasis. Our study, thus, opens exciting avenues to understand effects of ABPs on actin networks at a systems level in the future.

Materials and Methods

Plasmid construction

All plasmids used in this study are listed in Supplementary Table 1. Plasmids were constructed by assembling DNA fragments amplified by PCR into restriction endonuclease-digested vectors using NEB Hifi Builder (NewEngland BioLabs; cat.no: E2621L). The plasmids were confirmed with restriction digestion and sequencing.

Yeast Strains construction

All yeast strains used in this study are listed in Supplementary Table 2. S288c genetic background was used for all modifications. Yeast transformation was done using the Lithium Acetate based method as previously described[102]. Deletion and tagging of genes was done using the homologous recombination of PCR cassettes as described previously[103]. The strains were confirmed using colony PCR and fluorescence microscopy.

Live-cell Imaging of tropomyosin isoforms

Yeast strains were grown overnight in Synthetic Complete (SC) Media at 25°C. The overnight culture was used to inoculate a secondary culture which was allowed to grow till mid-log phase. The cells were then adhered on a Concanavalin A-coated glass-bottom dish (Cellvis cat: no: D35C4-20-1.5-N) containing SC media. Images were acquired using the Andor Dragonfly 502 spinning disk confocal system (Oxford Instruments) equipped with a fully-motorized Leica Dmi8 inverted microscope setup. Z-stacks were acquired using a 100x oil objective, captured with the Andor Sona scMOS camera and deconvolved using Andor Fusion software. The images were processed using Fiji and quantified using a previously described protocol[56,104].

Actin cable staining with phalloidin

In order to visualize the actin cables, cells were stained with Alexa488/Rhodamine Phalloidin and imaged using a previously described protocol[56,104]. Briefly, cells were grown at 23℃ until early-mid log phase in Yeast extract/Peptone/2%Glucose (YPD) media. The cells were then fixed twice with 4% paraformaldehyde in YPD and 4% paraformaldehyde in 1x PBS for 45 minutes each and washed thrice with 1x PBS. Rhodamine/Alexa488 phalloidin (Invitrogen cat: no: R415 and cat: no: A12379 respectively) was added to a final concentration of 0.4μM and incubated overnight with rotation at 4℃. Next day, the cells were washed thrice with 1X PBS. The cells were adhered on 6% Concanavalin A (Sigma cat: no: C2010) coated glass bottom dishes and z-stacks (step size = o.2μm, 31 slices) were acquired using Andor Dragonfly 502 Spinning Disk system and deconvolved using Andor Fusion Software.

480 **Actin and Tropomyosin Cable quantification**

481 Actin/Tropomyosin cable length and number was done exactly as previously described[104]. An exam-
482 ple of the quantification procedure and workflow are shown in **Figure. S7A**.

483

484 **Yeast mating experiment**

485 Yeast strains of opposite mating types were grown overnight at 25°C and mixed in equal ratio. The
486 mixture of the two strains were seeded on a 1.2% Agarose pad or on a 6% Concanavalin-A coated
487 glass bottom dish and allowed to grow at 25°C for 30-45 minutes. Time-lapse images were acquired
488 at an interval of 2 min to capture mating events.

489

490 **Purification and labeling of actin**

491 Rabbit skeletal muscle actin was purified from acetone powder generated from frozen ground hind
492 leg muscle tissue of young rabbits (PelFreez, USA). Lyophilized acetone powder stored at −80 °C
493 was mechanically sheared in a coffee grinder, resuspended in G-buffer (5 mM Tris-HCl pH 7.5,
494 0.5 mM Dithiothreitol (DTT), 0.2 mM ATP, and 0.1 mM $CaCl_2$), and cleared by centrifugation for 20 min
495 at 50,000 × g. The supernatant was collected and further filtered with the Whatman paper. Actin was
496 then polymerized overnight at 4 °C, slowly stirring, by the addition of 2 mM $MgCl_2$ and 50 mM NaCl to
497 the filtrate. Next morning, NaCl powder was added to a final concentration of 0.6 M, and stirring was
498 continued for another 30 min at 4 °C. F-actin was pelleted by centrifugation for 2.5 hrs at 280,000 ×
499 g. The pellet was solubilized by dounce homogenization and dialyzed against G-buffer for 48 h at
500 4 °C. Monomeric actin was precleared at 435,000 × g and loaded onto a Sephacryl S-200 16/60 gel-
501 filtration column (Cytiva, USA) equilibrated in G-Buffer. Fractions containing actin were stored at 4 °C.
502 To biotinylate actin, purified G-actin was first dialyzed overnight at 4 °C against G-buffer lacking DTT.
503 The monomeric actin was then polymerized by the addition of an equal volume of 2X labeling buffer
504 (50 mM imidazole pH 7.5, 200 mM KCl, 0.3 mM ATP, 4 mM $MgCl_2$). F-actin was then mixed with a
505 fivefold molar excess of NHS-XX-Biotin (Merck KGaA, Germany) and incubated in the dark for 15 h
506 at 4 °C. F-actin was pelleted by centrifugation at 450,000 × g for 40 min at room temperature, The
507 pellet was rinsed with G-buffer, homogenized with a dounce and dialyzed against G-buffer for 48 h at
508 4 °C. Biotinylated monomeric actin was purified further on a Sephacryl S-200 16/60 gel-filtration col-
509 umn as above. Aliquots of biotin-actin were snap-frozen in liquid N_2 and stored at −80 °C.
510 To fluorescently label actin, G-actin was polymerized by dialyzing overnight against modified F-buffer
511 (20 mM PIPES pH 6.9, 0.2 mM $CaCl_2$, 0.2 mM ATP, and 100 mM KCl). F-actin was incubated for 2 h
512 at room temperature with a fivefold molar excess of Alexa-488 NHS ester dye (Thermo Fisher Scien-
513 tific, USA, cat: no: A20100). F-actin was pelleted by centrifugation at 450,000 × g for 40 min at room
514 temperature, and the pellet was resuspended in G-buffer, homogenized with a dounce and further
515 incubated on ice for 2 h to depolymerize the filaments. The monomeric actin was then re-polymerized

516 on ice for 1 h by the addition of 100 mM KCl and 1 mM $MgCl_2$. F-actin was once again pelleted by
517 centrifugation for 40 min at 450,000 × g at 4 °C. The pellet was homogenized with a dounce and
518 dialyzed overnight at 4 °C against 1 L of G-buffer. Next morning, the solution was precleared by cen-
519 trifugation at 450,000 × g for 40 min at 4 °C. The supernatant was collected, and concentration and
520 labeling efficiency of actin were determined. Labelled actin was stored at 4 °C.
521
522 **Purification of profilin**
523 Human profilin-1 was expressed in *E. coli* strain BL21 (pRare) to log phase in LB broth at 37 °C and
524 induced with 1 mM IPTG for 3 h at 37 °C. Cells were then harvested by centrifugation at 15,000 × g
525 at 4 °C and stored at −80 °C. For purification, pellets were thawed and resuspended in 30 mL lysis
526 buffer (50 mM Tris-HCl pH 8, 1 mM DTT, 1 mM PMSF and protease inhibitors (0.5 µM each of pep-
527 statin A, antipain, leupeptin, aprotinin, and chymostatin), and the solution was sonicated on ice by a
528 tip sonicator. The lysate was centrifuged for 45 min at 120,000 × g at 4 °C. The supernatant was then
529 passed over 20 ml of Poly-L-proline conjugated beads in a disposable column (Bio-Rad, USA). The
530 beads were first washed at room temperature in wash buffer (10 mM Tris pH 8, 150 mM NaCl, 1 mM
531 EDTA, and 1 mM DTT) and then washed again with two column volumes of 10 mM Tris pH 8, 150 mM
532 NaCl, 1 mM EDTA, 1 mM DTT, and 3 M urea. Protein was then eluted with five column volumes of
533 10 mM Tris pH 8, 150 mM NaCl, 1 mM EDTA, 1 mM DTT, and 8 M urea. Pooled and concentrated
534 fractions were then dialyzed in 4 L of 2 mM Tris pH 8, 0.2 mM EGTA, 1 mM DTT, and 0.01% NaN3
535 for 4 h at 4 °C. The dialysis buffer was replaced with fresh 4 L buffer, and the dialysis was continued
536 overnight at 4 °C. The protein was centrifuged for 45 min at 450,000 × g at 4 °C, concentrated, ali-
537 quoted, flash-frozen in liquid N2, and stored at −80 °C.
538
539 **Purification of yeast and human Tpm isoforms**
540 All budding yeast and human tropomyosins were expressed in *E. coli* strain BL21 to log phase in LB
541 broth at 37 °C and induced with 1 mM IPTG for 3 h at 37 °C. Cells were then harvested by centrifuga-
542 tion at 15,000 × g at 4 °C and stored at −80 °C. For purification, pellets were thawed and resuspended
543 in 30 mL lysis buffer (20 mM Tris-HCl pH 7.5, 0.5 M NaCl, 5 mM $MgCl_2$, 1 mM PMSF, protease inhib-
544 itors (0.5 µM each of pepstatin A, antipain, leupeptin, aprotinin, and chymostatin)), and the solution
545 was sonicated on ice by a tip sonicator. The lysate was incubated at 80°C for 10 min in a water bath
546 and at room temperature for another 10 min. The lysate was centrifuged for 30 min at 30,000 x g at
547 4 °C, and the pellet was discarded. The protein was precipitated by adding 0.3M HCl to the superna-
548 tant till the pH reached 4.7. The solution was centrifuged for 30 min at 30,000 x g at 4°C. The pellet
549 was resuspended in 25 mL of wash buffer (100 mM Tris-HCl pH 7.5, 0.5 M NaCl, 5 mM $MgCl_2$, 1 mM
550 DTT). The acid precipitation and accompanying centrifugation step were repeated again. The pellet
551 was then resuspended in 25 mL of wash buffer and dialyzed in 2 L of dialysis buffer (20 mM HEPES
552 pH 6.8, 50 mM NaCl, 0.5 mM DTT) overnight at 4 °C. The dialyzed solution was loaded to a 5 ml

HiTrap Q HP column (Cytiva). The protein fractions were eluted with a linear gradient of NaCl (50–600 mM). The fractions were analyzed by SDS-PAGE to determine the ones containing Tpm. They were concentrated and further loaded on a Superose 6 gel-filtration column (Cytiva) pre-equilibrated with 20 mM Tris (pH 7.5), 50 mM KCl, 2 mM MgCl2, 1 mM DTT. Peak fractions were collected, concentrated, aliquoted, and flash-frozen in liquid N2 and stored at −80 °C.

Purification of yeast cofilin

His-tagged yeast Cof1 was expressed in *E. coli* strain BL21 to log phase in LB broth at 37 °C and induced with 1 mM IPTG for 3 h at 37 °C. Cells were then harvested by centrifugation at 15,000 × g at 4 °C and stored at −80 °C. For purification, pellets were thawed and resuspended in 30 mL lysis buffer (50 mM phosphate buffer pH 8, 20 mM Imidazole, 0.3 M NaCl, 1 mM PMSF, protease inhibitors), and the solution was sonicated on ice by a tip sonicator. The lysate was centrifuged for 45 min at 120,000 × g at 4 °C. The supernatant was incubated with 2 mL of washed Ni-NTA beads for 2 hrs at 4 °C. The solution was centrifuged at 1000 xg for 5 minutes. The supernatant was removed. The beads were washed 3 times with 10 mL of wash buffer (50 mM Phosphate buffer pH 8, 20 mM Imidazole, 0.3 M NaCl, 1 mM DTT) and subsequently centrifuged at 1000 xg for 2 min each time to remove the supernatant. Protein was then eluted with 1 mL of elution buffer (50 mM phosphate buffer pH 8, 250 mM Imidazole, 0.3 M NaCl, 1 mM DTT). Pooled and concentrated fractions were then loaded on a Superose 6 gel-filtration column (Cytiva) pre-equilibrated with 20 mM HEPES pH 7.5, 50 mM KCl, 0.5 mM DTT. Peak fractions were collected, concentrated, aliquoted, and flash-frozen in liquid N2 and stored at −80 °C.

TIRF microscopy

Glass coverslips (60 × 24 mm; Thermo Fisher Scientific, USA) were first cleaned by sonication in detergent for 20 min, followed by successive sonications in 1 M KOH, 1 M HCl, and ethanol for 20 min each. Coverslips were then washed extensively with H_2O and dried in an N_2 stream. The cleaned coverslips were coated with 2 mg/mL methoxy-polyethylene glycol (mPEG)-silane MW 2000 and 2 µg/mL biotin-PEG-silane MW 3400 (Laysan Bio, USA) in 80% ethanol (pH 2.0) and incubated overnight at 70 °C. Flow cells were assembled by rinsing PEG-coated coverslips with water, drying with N_2, and adhering to µ-Slide VI0.1 (0.1 mm × 17 mm × 1 mm) flow chambers (Ibidi, Germany) with double-sided tape (2.5 cm × 2 mm × 120 µm) and epoxy resin for 5 min (Devcon, USA). Before each reaction, the flow cell was sequentially incubated for 1 min each with 4 µg/ml streptavidin and 1% BSA in 20 mM HEPES pH 7.5 and 50 mM KCl. The flow cell was then equilibrated with TIRF buffer (10 mM imidazole, pH 7.4, 50 mM KCl, 1 mM $MgCl_2$, 1 mM EGTA, 0.2 mM ATP, 10 mM DTT, 2 mM DABCO, and 0.5% methylcellulose [4000 cP]).

Actin filaments were assembled by introducing 1 µM 15% Alexa 488 labelled 0.1% biotinylated actin and 2 µM profilin in the flow cell, with or without 10 µM Tpm. Filaments were allowed to grow for 2 to

590 3 min. For experiments containing Tpm, the flow cell was then rinsed with TIRF buffer supplemented
591 with 10 μM Tpm to remove free actin. The solution was then replaced with 10 μM Tpm and 150 nM
592 Cof1. For control experiments containing no Tpm, both washing and cofilin addition step had no Tpm
593 in the solution.
594
595 **Image acquisition and analysis**
596 Single-wavelength time-lapse TIRF imaging was performed on a Nikon-Ti2000 inverted microscope
597 equipped with a 40 mW Argon laser, a 60X TIRF-objective with a numerical aperture of 1.49 (Nikon
598 Instruments Inc., USA), and an IXON LIFE 888 EMCCD camera (Andor Ixon, UK). One pixel was
599 equivalent to 144 × 144 nm. Focus was maintained by the Perfect Focus system (Nikon Instruments
600 Inc., Japan). Time-lapse images were acquired every 2 s using Nikon Elements imaging software
601 (Nikon Instruments Inc., Japan). The sample was excited by a 488 nm laser for imaging. Images were
602 analyzed in Fiji. Normalized rates of severing by cofilin, in the presence or absence of different Tpm
603 isoforms, were determined by counting the number of severing events as a function of time in a field
604 of view divided by the total length of all filaments in the field of view. The average filament length due
605 to severing was measured ~2 min after the cofilin flow-in. Data analysis and curve fitting was carried
606 out in Microcal Origin.
607
608 **RNA extraction and RT-qPCR**
609 Hot phenol method was used to extract RNA from yeast cells[105]. Overnight grown yeast cells were
610 diluted and allowed to grow until OD at 600nm reached 1. Cells were treated with equal volumes of
611 TES and water saturated acidic phenol and precipitated at -80℃ to extract RNA. The extracted RNA
612 was then treated with DNAse A and this was used as a template for first strand cDNA synthesis.
613 Following this, qRT-PCR was set up using the cDNA to check the expression levels. Gene specific
614 primers were used to assess the Tpm1 and Tpm2 levels in wild type and different mutant background.
615 TDH1 and PGK1 housekeeping genes were used as controls for all qRT-PCR experiments.
616
617 **Vesicle delivery to bud**
618 Vesicle delivery was visualized using an N-terminal tagged ymScarleti-Sec4 construct expressed un-
619 der ADH promoter as an additional copy integrated into the *ura3* locus. Overnight grown yeast cells
620 were diluted and allowed to grow until mid-log phase. Cells were adhered on a Concanavalin A-coated
621 glass bottom dish and z-stacks were acquired with a step size of 0.5μm to cover a range of 6μm. The
622 ratio of ymScarleti-Sec4 intensity in the bud and mother were taken and plotted to assess targeting
623 of vesicles to the bud via the actin cable network. Images were also acquired using Andor BC43 table-
624 top spinning disk confocal system using a 60x oil objective and scMOS camera detection. Images
625 were deconvolved using Andor Fusion software and any adjustments for representation were done
626 using Fiji (ImageJ)[106].

627

628 **Mitochondrial morphology**

629 Mitochondrial morphology was assessed with Om45-3xmCherry tagged at its genomic locus or Su9-
630 mNeonGreen expressed from an integrated plasmid as a mitochondrial marker during imaging. Z-
631 stacks of mid-log phase cells were acquired using Olympus IX83 widefield fluorescence microscope
632 system and images were processed using the Mitochondria Analyzer plug-in in Fiji[106] to quantify
633 mitochondrial morphology. An example of the quantification procedure and details of parameters used
634 for segmentation of mitochondria are shown in **Fig. S7B**.

635

636 **Actin patch imaging**

637 Actin patch lifetime was measured using LifeAct-eGFP as an actin patch marker. Time-lapse images
638 of LifeAct-eGFP expressing cells were acquired at an interval of 0.5 sec for 120 cycles with a 100x
639 oil objective using Olympus SpinSR spinning disk confocal system. Patch lifetime was calculated as
640 the time between appearance and disappearance of LifeAct-eGFP patch fluorescence signal. Imag

641

642 **Retrograde Actin Cable Flow**

643 Retrograde actin cable flow was assessed using LifeAct-eGFP as an actin cable marker. Time-lapse
644 images of LifeAct-eGFP expressing cells were acquired at an interval of 1 sec for 20 cycles with a
645 100x oil objective using Olympus SpinSR spinning disk confocal system. Images were analyzed to
646 measure rate of actin cable elongation towards the rear of the mother cell.

647

648 **Latrunculin B sensitivity assay**

649 Yeast cells were grown to mid-log phase at 25°C and LatB (SigmaAldrich, cat. No.: 428020) was
650 added to a final concentration of 67μM. Cells were fixed with 4% paraformaldehyde at time points 0
651 min, 2 min and 04.30 min after LatB addition. The cells were then stained with Alexa488-phalloidin
652 and imaged as described above.

653

654 **Image analysis and statistical analysis**

655 All images were processed using Fiji (ImageJ)[106]. The specific analysis pipelines are mentioned in
656 the above sections for each type of measurement. The graphs were plotted using GraphPad Prism
657 (v.6.04) and statistical tests were also performed using in-built functions in GraphPad Prism. * $p <$
658 0.05, ** $p < 0.01$, *** $p < 0.001$, ****$p < 0.0001$

659

Acknowledgements

We thank the Department of Biochemistry, Indian Institute of Science for access to DST-FIST imaging and other central facilities. We also thank the Divisional Bioimaging Facility. We are grateful to Mr. Pabitra Sharma for help with image analysis. We thank Prof. PN Rangarajan, Prof. Ramanujam Srinivasan, Prof. Sunil Laxman, Prof. Sachin Kotak, Prof. Sunish Radhakrishnan, and Prof. Marko Kaksonen for their feedback on the manuscript. AD and JK acknowledge GATE fellowship from IISc. JSB acknowledges KVPY fellowship from IISc. We thank Silvia Jansen for advice on quantification of TIRF microscopy experiments and Blake Miller for help with protein purification.

Author Contributions

SP and AD conceived and supervised the experiments. AD and BVT constructed yeast strains and expression plasmids. AD and BVT performed experiments and data analysis. AS made yeast strains and performed data analysis. JK made the plasmid constructs for protein purification, performed western blotting, and data analysis. SB purified proteins and performed *in-vitro* reconstitution experiments, and data analysis. SS conceived and supervised the in-vitro experiments with purified proteins. JSB performed data analysis. SP, SS, AD and BVT wrote the manuscript, and all the authors helped in editing the manuscript.

Funding

This work was financially supported by a Department of Biotechnology-Wellcome Trust India Alliance intermediate fellowship (IA/I/21/1/505633), SERB SRG grant (SRG/2021/001600) and an Indian Institute of Science (IISc) start-up grant awarded to S.P. S.S. is supported by NIH NIGMS grant R35GM143050.

Competing interest statement

The authors declare no conflict of interest.

References

1. Pruyne, D. (2008). Tropomyosin Function in Yeast. In Tropomyosin, P. Gunning, ed. (Springer), pp. 168–186. https://doi.org/10.1007/978-0-387-85766-4_14.

2. Gunning, P., O'Neill, G., and Hardeman, E. (2008). Tropomyosin-based regulation of the actin cytoskeleton in time and space. Physiol Rev *88*, 1–35. https://doi.org/10.1152/physrev.00001.2007.

3. Hitchcock-DeGregori, S.E., and Barua, B. (2017). Tropomyosin Structure, Function, and Interactions: A Dynamic Regulator. Subcell Biochem *82*, 253–284. https://doi.org/10.1007/978-3-319-49674-0_9.

4. Gunning, P.W., Hardeman, E.C., Lappalainen, P., and Mulvihill, D.P. (2015). Tropomyosin - master regulator of actin filament function in the cytoskeleton. J Cell Sci *128*, 2965–2974. https://doi.org/10.1242/jcs.172502.

5. von der Ecken, J., Müller, M., Lehman, W., Manstein, D.J., Penczek, P.A., and Raunser, S. (2015). Structure of the F-actin–tropomyosin complex. Nature *519*, 114–117. https://doi.org/10.1038/nature14033.

6. Obeidy, P., Sobey, T., Nicovich, P.R., Coster, A.C.F., and Pandzic, E. (2021). Tropomyosin isoforms segregate into distinct clusters on single actin filaments (Biophysics) https://doi.org/10.1101/2021.07.23.453476.

7. Bailey, K. (1953). The Structure of Tropomyosin. Proceedings of the Royal Society of London. Series B, Biological Sciences *141*, 45–48.

8. Cohen, C., and Longley, W. (1966). Tropomyosin Paracrystals Formed by Divalent Cations. Science *152*, 794–796. https://doi.org/10.1126/science.152.3723.794.

9. Bailey, K. (1946). Tropomyosin: a New Asymmetric Protein Component of Muscle. Nature *157*, 368–369. https://doi.org/10.1038/157368b0.

10. McKillop, D.F., and Geeves, M.A. (1993). Regulation of the interaction between actin and myosin subfragment 1: evidence for three states of the thin filament. Biophys J *65*, 693–701.

11. Marston, S., and El-Mezgueldi, M. (2008). Role of Tropomyosin in the Regulation of Contraction in Smooth Muscle. In Tropomyosin, P. Gunning, ed. (Springer), pp. 110–123. https://doi.org/10.1007/978-0-387-85766-4_9.

12. Manstein, D.J., Meiring, J.C.M., Hardeman, E.C., and Gunning, P.W. (2020). Actin–tropomyosin distribution in non-muscle cells. J Muscle Res Cell Motil *41*, 11–22. https://doi.org/10.1007/s10974-019-09514-0.

13. Balasubramanian, M.K., Helfman, D.M., and Hemmingsen, S.M. (1992). A new tropomyosin essential for cytokinesis in the fission yeast S. pombe. Nature *360*, 84–87. https://doi.org/10.1038/360084a0.

14. Vrhovski, B., Thézé, N., and Thiébaud, P. (2008). Structure and evolution of tropomyosin genes. Adv Exp Med Biol *644*, 6–26. https://doi.org/10.1007/978-0-387-85766-4_2.

15. Liu, H.P., and Bretscher, A. (1989). Disruption of the single tropomyosin gene in yeast results in the disappearance of actin cables from the cytoskeleton. Cell *57*, 233–242. https://doi.org/10.1016/0092-8674(89)90961-6.

16. Drees, B., Brown, C., Barrell, B.G., and Bretscher, A. (1995). Tropomyosin is essential in yeast, yet the TPM1 and TPM2 products perform distinct functions. J Cell Biol *128*, 383–392. https://doi.org/10.1083/jcb.128.3.383.

17. Bernstein, B.W., and Bamburg, J.R. (1982). Tropomyosin binding to F-actin protects the F-actin from disassembly by brain actin-depolymerizing factor (ADF). Cell Motility *2*, 1–8. https://doi.org/10.1002/cm.970020102.

18. Ono, S., and Ono, K. (2002). Tropomyosin inhibits ADF/cofilin-dependent actin filament dynamics. J Cell Biol *156*, 1065–1076. https://doi.org/10.1083/jcb.200110013.

19. Robaszkiewicz, K., Ostrowska, Z., Marchlewicz, K., and Moraczewska, J. (2016). Tropomyosin isoforms differentially modulate the regulation of actin filament polymerization and depolymerization by cofilins. The FEBS Journal *283*, 723–737. https://doi.org/10.1111/febs.13626.

20. Goode, B.L., Eskin, J., and Shekhar, S. (2023). Mechanisms of actin disassembly and turnover. J Cell Biol *222*, e202309021. https://doi.org/10.1083/jcb.202309021.

21. Brayford, S., Bryce, N.S., Schevzov, G., Haynes, E.M., Bear, J.E., Hardeman, E.C., and Gunning, P.W. (2016). Tropomyosin Promotes Lamellipodial Persistence by Collaborating with Arp2/3 at the Leading Edge. Curr Biol *26*, 1312–1318. https://doi.org/10.1016/j.cub.2016.03.028.

22. Pruyne, D.W., Schott, D.H., and Bretscher, A. (1998). Tropomyosin-containing actin cables direct the Myo2p-dependent polarized delivery of secretory vesicles in budding yeast. J Cell Biol *143*, 1931–1945. https://doi.org/10.1083/jcb.143.7.1931.

23. Geeves, M.A., Hitchcock-DeGregori, S.E., and Gunning, P.W. (2015). A systematic nomenclature for mammalian tropomyosin isoforms. J Muscle Res Cell Motil *36*, 147–153. https://doi.org/10.1007/s10974-014-9389-6.

24. Reindl, T., Giese, S., Greve, J.N., Reinke, P.Y., Chizhov, I., Latham, S.L., Mulvihill, D.P., Taft, M.H., and Manstein, D.J. (2022). Distinct actin–tropomyosin cofilament populations drive the functional diversification of cytoskeletal myosin motor complexes. iScience *25*, 104484. https://doi.org/10.1016/j.isci.2022.104484.

25. Palani, S., Köster, D.V., Hatano, T., Kamnev, A., Kanamaru, T., Brooker, H.R., Hernandez-Fernaud, J.R., Jones, A.M.E., Millar, J.B.A., Mulvihill, D.P., et al. (2019). Phosphoregulation of tropomyosin is crucial for actin cable turnover and division site placement. J Cell Biol *218*, 3548–3559. https://doi.org/10.1083/jcb.201809089.

26. Boiero Sanders, M., Antkowiak, A., and Michelot, A. (2020). Diversity from similarity: cellular strategies for assigning particular identities to actin filaments and networks. Open Biology *10*, 200157. https://doi.org/10.1098/rsob.200157.

27. Tojkander, S., Gateva, G., Schevzov, G., Hotulainen, P., Naumanen, P., Martin, C., Gunning, P.W., and Lappalainen, P. (2011). A molecular pathway for myosin II recruitment to stress fibers. Curr Biol *21*, 539–550. https://doi.org/10.1016/j.cub.2011.03.007.

28. Kee, A.J., Yang, L., Lucas, C.A., Greenberg, M.J., Martel, N., Leong, G.M., Hughes, W.E., Cooney, G.J., James, D.E., Ostap, E.M., et al. (2015). An Actin Filament Population Defined by the Tropomyosin Tpm3.1 Regulates Glucose Uptake. Traffic *16*, 691–711. https://doi.org/10.1111/tra.12282.

29. Bach, C.T.T., Creed, S., Zhong, J., Mahmassani, M., Schevzov, G., Stehn, J., Cowell, L.N., Naumanen, P., Lappalainen, P., Gunning, P.W., et al. (2009). Tropomyosin Isoform Expression Regulates the Transition of Adhesions To Determine Cell Speed and Direction. Molecular and Cellular Biology *29*, 1506–1514. https://doi.org/10.1128/MCB.00857-08.

30. Meiring, J.C.M., Bryce, N.S., Niño, J.L.G., Gabriel, A., Tay, S.S., Hardeman, E.C., Biro, M., and Gunning, P.W. (2019). Tropomyosin concentration but not formin nucleators mDia1 and mDia3 determines the level of tropomyosin incorporation into actin filaments. Sci Rep *9*, 6504. https://doi.org/10.1038/s41598-019-42977-2.

31. Johnson, M., East, D.A., and Mulvihill, D.P. (2014). Formins Determine the Functional Properties of Actin Filaments in Yeast. Current Biology *24*, 1525–1530. https://doi.org/10.1016/j.cub.2014.05.034.

32. Zhao, S., Cai, J., Zhang, X., Cui, J., and Jiu, Y. (2020). Different formins restrict localization of distinct tropomyosins on dorsal stress fibers in osteosarcoma cells. Cytoskeleton *77*, 16–24. https://doi.org/10.1002/cm.21588.

33. Gateva, G., Kremneva, E., Reindl, T., Kotila, T., Kogan, K., Gressin, L., Gunning, P.W., Manstein, D.J., Michelot, A., and Lappalainen, P. (2017). Tropomyosin Isoforms Specify Functionally Distinct Actin Filament Populations In Vitro. Current Biology *27*, 705–713. https://doi.org/10.1016/j.cub.2017.01.018.

766 34. Selvaraj, M., Kokate, S.B., Reggiano, G., Kogan, K., Kotila, T., Kremneva, E., DiMaio, F., Lappalainen, P., and
767 Huiskonen, J.T. (2023). Structural basis underlying specific biochemical activities of non-muscle tropomyosin
768 isoforms. Cell Reports *42*, 111900. https://doi.org/10.1016/j.celrep.2022.111900.

769 35. Kumari, R., Ven, K., Chastney, M., Peränen, J., Aaron, J., Almeida-Souza, L., Kremneva, E., Poincloux, R., Chew,
770 T.-L., Gunning, P.W., et al. (2023). Specialized actin nanoscale layers control focal adhesion turnover. Preprint
771 at bioRxiv, https://doi.org/10.1101/2023.02.15.528622 https://doi.org/10.1101/2023.02.15.528622.

772 36. Alioto, S.L., Garabedian, M.V., Bellavance, D.R., and Goode, B.L. (2016). Tropomyosin and Profilin Cooperate
773 to Promote Formin-Mediated Actin Nucleation and Drive Yeast Actin Cable Assembly. Curr Biol *26*, 3230–3237.
774 https://doi.org/10.1016/j.cub.2016.09.053.

775 37. Okada, K., Ravi, H., Smith, E.M., and Goode, B.L. (2006). Aip1 and Cofilin Promote Rapid Turnover of Yeast
776 Actin Patches and Cables: A Coordinated Mechanism for Severing and Capping Filaments. Mol Biol Cell *17*,
777 2855–2868. https://doi.org/10.1091/mbc.E06-02-0135.

778 38. Chaudhry, F., Breitsprecher, D., Little, K., Sharov, G., Sokolova, O., and Goode, B.L. (2013). Srv2/cyclase-associ-
779 ated protein forms hexameric shurikens that directly catalyze actin filament severing by cofilin. Mol Biol Cell
780 *24*, 31–41. https://doi.org/10.1091/mbc.E12-08-0589.

781 39. Huckaba, T.M., Lipkin, T., and Pon, L.A. (2006). Roles of type II myosin and a tropomyosin isoform in retrograde
782 actin flow in budding yeast. J Cell Biol *175*, 957–969. https://doi.org/10.1083/jcb.200609155.

783 40. Higuchi, R., Vevea, J.D., Swayne, T.C., Chojnowski, R., Hill, V., Boldogh, I.R., and Pon, L.A. (2013). Actin Dy-
784 namics Affect Mitochondrial Quality Control and Aging in Budding Yeast. Current Biology *23*, 2417–2422.
785 https://doi.org/10.1016/j.cub.2013.10.022.

786 41. Hodges, A.R., Krementsova, E.B., Bookwalter, C.S., Fagnant, P.M., Sladewski, T.E., and Trybus, K.M. (2012).
787 Tropomyosin is essential for processive movement of a class V myosin from budding yeast. Curr Biol *22*, 1410–
788 1416. https://doi.org/10.1016/j.cub.2012.05.035.

789 42. Altmann, K., Frank, M., Neumann, D., Jakobs, S., and Westermann, B. (2008). The class V myosin motor protein,
790 Myo2, plays a major role in mitochondrial motility in Saccharomyces cerevisiae. The Journal of Cell Biology *181*,
791 119. https://doi.org/10.1083/jcb.200709099.

792 43. Johnston, G.C., Prendergast, J.A., and Singer, R.A. (1991). The Saccharomyces cerevisiae MYO2 gene encodes
793 an essential myosin for vectorial transport of vesicles. J Cell Biol *113*, 539–551.
794 https://doi.org/10.1083/jcb.113.3.539.

795 44. Hatano, T., Lim, T.C., Billault-Chaumartin, I., Dhar, A., Gu, Y., Massam-Wu, T., Scott, W., Adishesha, S., Chapa-
796 y-Lazo, B., Springall, L., et al. (2022). mNG-tagged fusion proteins and nanobodies to visualize tropomyosins in
797 yeast and mammalian cells. Journal of Cell Science *135*, jcs260288. https://doi.org/10.1242/jcs.260288.

798 45. Coulton, A.T., East, D.A., Galinska-Rakoczy, A., Lehman, W., and Mulvihill, D.P. (2010). The recruitment of
799 acetylated and unacetylated tropomyosin to distinct actin polymers permits the discrete regulation of specific
800 myosins in fission yeast. J Cell Sci *123*, 3235–3243. https://doi.org/10.1242/jcs.069971.

801 46. Brooker, H.R., Geeves, M.A., and Mulvihill, D.P. (2016). Analysis of biophysical and functional consequences of
802 tropomyosin–fluorescent protein fusions. FEBS Letters *590*, 3111–3121. https://doi.org/10.1002/1873-
803 3468.12346.

804 47. Polevoda, B., Cardillo, T.S., Doyle, T.C., Bedi, G.S., and Sherman, F. (2003). Nat3p and Mdm20p Are Required
805 for Function of Yeast NatB Nα-terminal Acetyltransferase and of Actin and Tropomyosin*. Journal of Biological
806 Chemistry *278*, 30686–30697. https://doi.org/10.1074/jbc.M304690200.

48. Singer, J.M., and Shaw, J.M. (2003). Mdm20 protein functions with Nat3 protein to acetylate Tpm1 protein and regulate tropomyosin–actin interactions in budding yeast. Proceedings of the National Academy of Sciences *100*, 7644–7649. https://doi.org/10.1073/pnas.1232343100.

49. Maytum, R., Geeves, M.A., and Konrad, M. (2000). Actomyosin regulatory properties of yeast tropomyosin are dependent upon N-terminal modification. Biochemistry *39*, 11913–11920. https://doi.org/10.1021/bi000977g.

50. Monteiro, P.B., Lataro, R.C., Ferro, J.A., and Reinach, F. de C. (1994). Functional alpha-tropomyosin produced in Escherichia coli. A dipeptide extension can substitute the amino-terminal acetyl group. J Biol Chem *269*, 10461–10466.

51. Greenfield, N.J., Stafford, W.E., and Hitchcock-Degregori, S.E. (1994). The effect of N-terminal acetylation on the structure of an N-terminal tropomyosin peptide and αα-tropomyosin. Protein Science *3*, 402–410. https://doi.org/10.1002/pro.5560030304.

52. Christensen, J.R., Hocky, G.M., Homa, K.E., Morganthaler, A.N., Hitchcock-DeGregori, S.E., Voth, G.A., and Kovar, D.R. (2017). Competition between Tropomyosin, Fimbrin, and ADF/Cofilin drives their sorting to distinct actin filament networks. eLife *6*, e23152. https://doi.org/10.7554/eLife.23152.

53. Simon, V. r., Karmon, S. l., and Pon, L. a. (1997). Mitochondrial inheritance: Cell cycle and actin cable dependence of polarized mitochondrial movements in Saccharomyces cerevisiae. Cell Motility *37*, 199–210. https://doi.org/10.1002/(SICI)1097-0169(1997)37:3<199::AID-CM2>3.0.CO;2-2.

54. Drubin, D.G., Jones, H.D., and Wertman, K.F. (1993). Actin structure and function: roles in mitochondrial organization and morphogenesis in budding yeast and identification of the phalloidin-binding site. Mol Biol Cell *4*, 1277–1294. https://doi.org/10.1091/mbc.4.12.1277.

55. McInally, S.G., Reading, A.J.B., Rosario, A., Jelenkovic, P.R., Goode, B.L., and Kondev, J. (2024). Length control emerges from cytoskeletal network geometry. Proceedings of the National Academy of Sciences *121*, e2401816121. https://doi.org/10.1073/pnas.2401816121.

56. McInally, S.G., Kondev, J., and Goode, B.L. (2021). Scaling of subcellular actin structures with cell length through decelerated growth. Elife *10*, e68424. https://doi.org/10.7554/eLife.68424.

57. Janco, M., Bonello, T.T., Byun, A., Coster, A.C.F., Lebhar, H., Dedova, I., Gunning, P.W., and Böcking, T. (2016). The impact of tropomyosins on actin filament assembly is isoform specific. Bioarchitecture *6*, 61–75. https://doi.org/10.1080/19490992.2016.1201619.

58. Bryce, N.S., Schevzov, G., Ferguson, V., Percival, J.M., Lin, J.J.-C., Matsumura, F., Bamburg, J.R., Jeffrey, P.L., Hardeman, E.C., Gunning, P., et al. (2003). Specification of actin filament function and molecular composition by tropomyosin isoforms. Mol Biol Cell *14*, 1002–1016. https://doi.org/10.1091/mbc.e02-04-0244.

59. Percival, J.M., Hughes, J.A.I., Brown, D.L., Schevzov, G., Heimann, K., Vrhovski, B., Bryce, N., Stow, J.L., and Gunning, P.W. (2004). Targeting of a Tropomyosin Isoform to Short Microfilaments Associated with the Golgi Complex. MBoC *15*, 268–280. https://doi.org/10.1091/mbc.e03-03-0176.

60. Goins, L.M., and Mullins, R.D. (2015). A novel tropomyosin isoform functions at the mitotic spindle and Golgi in Drosophila. Mol Biol Cell *26*, 2491–2504. https://doi.org/10.1091/mbc.E14-12-1619.

61. Veeranan-Karmegam, R., Boggupalli, D.P., Liu, G., and Gonsalvez, G.B. (2016). A new isoform of Drosophila non-muscle Tropomyosin 1 interacts with Kinesin-1 and functions in oskar mRNA localization. J Cell Sci *129*, 4252–4264. https://doi.org/10.1242/jcs.194332.

62. Martin, C., Schevzov, G., and Gunning, P. (2010). Alternatively spliced N-terminal exons in tropomyosin isoforms do not act as autonomous targeting signals. J Struct Biol *170*, 286–293. https://doi.org/10.1016/j.jsb.2009.12.016.

63. Gonzalez Rodriguez, S., Wirshing, A.C.E., Goodman, A.L., and Goode, B.L. (2023). Cytosolic concentrations of actin binding proteins and the implications for in vivo F-actin turnover. J Cell Biol *222*, e202306036. https://doi.org/10.1083/jcb.202306036.

64. Sagot, I., Klee, S.K., and Pellman, D. (2002). Yeast formins regulate cell polarity by controlling the assembly of actin cables. Nat Cell Biol *4*, 42–50. https://doi.org/10.1038/ncb719.

65. Evangelista, M., Pruyne, D., Amberg, D.C., Boone, C., and Bretscher, A. (2002). Formins direct Arp2/3-independent actin filament assembly to polarize cell growth in yeast. Nat Cell Biol *4*, 32–41. https://doi.org/10.1038/ncb718.

66. Pruyne, D., Gao, L., Bi, E., and Bretscher, A. (2004). Stable and Dynamic Axes of Polarity Use Distinct Formin Isoforms in Budding Yeast. MBoC *15*, 4971–4989. https://doi.org/10.1091/mbc.e04-04-0296.

67. Buttery, S.M., Yoshida, S., and Pellman, D. (2007). Yeast Formins Bni1 and Bnr1 Utilize Different Modes of Cortical Interaction during the Assembly of Actin Cables. Mol Biol Cell *18*, 1826–1838. https://doi.org/10.1091/mbc.E06-09-0820.

68. Bretscher, A. (2013). Deconstructing formin-dependent actin cable assembly. Proceedings of the National Academy of Sciences *110*, 18744–18745. https://doi.org/10.1073/pnas.1318683110.

69. Wirshing, A.C.E., and Goode, B.L. (2024). Improved tools for live imaging of F-actin structures in yeast. MBoC *35*, mr7. https://doi.org/10.1091/mbc.E24-05-0212-T.

70. Evangelista, M., Blundell, K., Longtine, M.S., Chow, C.J., Adames, N., Pringle, J.R., Peter, M., and Boone, C. (1997). Bni1p, a Yeast Formin Linking Cdc42p and the Actin Cytoskeleton During Polarized Morphogenesis. Science *276*, 118–122. https://doi.org/10.1126/science.276.5309.118.

71. Matheos, D., Metodiev, M., Muller, E., Stone, D., and Rose, M.D. (2004). Pheromone-induced polarization is dependent on the Fus3p MAPK acting through the formin Bni1p. J Cell Biol *165*, 99–109. https://doi.org/10.1083/jcb.200309089.

72. Soohey, S. (2017). Role of G-protein Regulation of Formins during Gradient Tracking in Saccharomyces cerevisiae.

73. Merlini, L., Dudin, O., and Martin, S.G. (2013). Mate and fuse: how yeast cells do it. Open Biology *3*, 130008. https://doi.org/10.1098/rsob.130008.

74. Hašek, J., Rupeš, I., Svobodová, J., and Streiblová, E. (1987). Tubulin and Actin Topology during Zygote Formation of Saccharomyces cerevisiae. Microbiology *133*, 3355–3363. https://doi.org/10.1099/00221287-133-12-3355.

75. Liu, H., and Bretscher, A. (1992). Characterization of TPM1 disrupted yeast cells indicates an involvement of tropomyosin in directed vesicular transport. J Cell Biol *118*, 285–299. https://doi.org/10.1083/jcb.118.2.285.

76. Magliozzi, J.O., Rands, T.J., Shrestha, S., Simke, W.C., Hase, N.E., Juanes, M.A., Kelley, J.B., and Goode, B.L. (2024). The roles of yeast formins and their regulators Bud6 and Bil2 in the pheromone response. Mol Biol Cell *35*, ar85. https://doi.org/10.1091/mbc.E23-11-0459.

77. Smith, B.A., Gelles, J., and Goode, B.L. (2014). Single-Molecule Studies of Actin Assembly and Disassembly Factors. Methods Enzymol *540*, 95–117. https://doi.org/10.1016/B978-0-12-397924-7.00006-6.

78. Shekhar, S., and Carlier, M.-F. (2016). Single-filament kinetic studies provide novel insights into regulation of actin-based motility. MBoC *27*, 1–6. https://doi.org/10.1091/mbc.E15-06-0352.

79. Jansen, S., and Goode, B.L. (2019). Tropomyosin isoforms differentially tune actin filament length and disassembly. MBoC *30*, 671–679. https://doi.org/10.1091/mbc.E18-12-0815.

80. Lazzarino, D.A., Boldogh, I., Smith, M.G., Rosand, J., and Pon, L.A. (1994). Yeast mitochondria contain ATP-sensitive, reversible actin-binding activity. Mol Biol Cell *5*, 807–818. https://doi.org/10.1091/mbc.5.7.807.

81. Boldogh, I.R., and Pon, L.A. (2006). Interactions of mitochondria with the actin cytoskeleton. Biochim Biophys Acta *1763*, 450–462. https://doi.org/10.1016/j.bbamcr.2006.02.014.

82. Liu, B., Larsson, L., Caballero, A., Hao, X., Öling, D., Grantham, J., and Nyström, T. (2010). The Polarisome Is Required for Segregation and Retrograde Transport of Protein Aggregates. Cell *140*, 257–267. https://doi.org/10.1016/j.cell.2009.12.031.

83. Liu, B., Larsson, L., Franssens, V., Hao, X., Hill, S.M., Andersson, V., Höglund, D., Song, J., Yang, X., Öling, D., et al. (2011). Segregation of protein aggregates involves actin and the polarity machinery. Cell *147*, 959–961. https://doi.org/10.1016/j.cell.2011.11.018.

84. Yang, H.-C., and Pon, L.A. (2002). Actin cable dynamics in budding yeast. Proceedings of the National Academy of Sciences *99*, 751–756. https://doi.org/10.1073/pnas.022462899.

85. Dua, N., Seshadri, A., and Badrinarayanan, A. (2022). DarT-mediated mtDNA damage induces dynamic reorganization and selective segregation of mitochondria. J Cell Biol *221*, e202205104. https://doi.org/10.1083/jcb.202205104.

86. Riedl, J., Crevenna, A.H., Kessenbrock, K., Yu, J.H., Neukirchen, D., Bista, M., Bradke, F., Jenne, D., Holak, T.A., Werb, Z., et al. (2008). Lifeact: a versatile marker to visualize F-actin. Nat Methods *5*, 605–607. https://doi.org/10.1038/nmeth.1220.

87. Skau, C.T., and Kovar, D.R. (2010). Fimbrin and Tropomyosin Competition Regulates Endocytosis and Cytokinesis Kinetics in Fission Yeast. Current Biology *20*, 1415–1422. https://doi.org/10.1016/j.cub.2010.06.020.

88. Burke, T.A., Christensen, J.R., Barone, E., Suarez, C., Sirotkin, V., and Kovar, D.R. (2014). Homeostatic actin cytoskeleton networks are regulated by assembly factor competition for monomers. Curr Biol *24*, 579–585. https://doi.org/10.1016/j.cub.2014.01.072.

89. Wirshing, A.C.E., Rodriguez, S.G., and Goode, B.L. (2023). Evolutionary tuning of barbed end competition allows simultaneous construction of architecturally distinct actin structures. J Cell Biol *222*, e202209105. https://doi.org/10.1083/jcb.202209105.

90. Antkowiak, A., Guillotin, A., Sanders, M.B., Colombo, J., Vincentelli, R., and Michelot, A. (2019). Sizes of actin networks sharing a common environment are determined by the relative rates of assembly. PLOS Biology *17*, e3000317. https://doi.org/10.1371/journal.pbio.3000317.

91. Michelot, A., and Drubin, D.G. (2011). Building Distinct Actin Filament Networks in a Common Cytoplasm. Current Biology *21*, R560–R569. https://doi.org/10.1016/j.cub.2011.06.019.

92. Young, M.E., Cooper, J.A., and Bridgman, P.C. (2004). Yeast actin patches are networks of branched actin filaments. Journal of Cell Biology *166*, 629–635. https://doi.org/10.1083/jcb.200404159.

93. Winter, D., Podtelejnikov, A.V., Mann, M., and Li, R. (1997). The complex containing actin-related proteins Arp2 and Arp3 is required for the motility and integrity of yeast actin patches. Curr Biol *7*, 519–529. https://doi.org/10.1016/s0960-9822(06)00223-5.

94. Karpova, T.S., McNally, J.G., Moltz, S.L., and Cooper, J.A. (1998). Assembly and function of the actin cytoskeleton of yeast: relationships between cables and patches. J Cell Biol *142*, 1501–1517. https://doi.org/10.1083/jcb.142.6.1501.

95. Pelham, R.J., and Chang, F. (2001). Role of actin polymerization and actin cables in actin-patch movement in Schizosaccharomyces pombe. Nat Cell Biol *3*, 235–244. https://doi.org/10.1038/35060020.

96. Okada, H., MacTaggart, B., Ohya, Y., and Bi, E. (2021). The kinetic landscape and interplay of protein networks in cytokinesis. iScience *24*, 101917. https://doi.org/10.1016/j.isci.2020.101917.

97. Frye, J., Klenchin, V.A., and Rayment, I. (2010). Structure of the Tropomyosin Overlap Complex from Chicken Smooth Muscle: Insight into the Diversity of N-Terminus Recognition. Biochemistry *49*, 4908–4920. https://doi.org/10.1021/bi100349a.

98. Tang, Q., Pollard, L.W., Homa, K.E., Kovar, D.R., and Trybus, K.M. (2023). Acetylation of fission yeast tropomyosin does not promote differential association with cognate formins. Cytoskeleton *80*, 77–92. https://doi.org/10.1002/cm.21745.

99. Shin, M., van Leeuwen, J., Boone, C., and Bretscher, A. (2018). Yeast Aim21/Tda2 both regulates free actin by reducing barbed end assembly and forms a complex with Cap1/Cap2 to balance actin assembly between patches and cables. Mol Biol Cell *29*, 923–936. https://doi.org/10.1091/mbc.E17-10-0592.

100. Hsiao, J., Goins, L., Petek, N., and Mullins, R. (2015). Arp2/3 Complex and Cofilin Modulate Binding of Tropomyosin to Branched Actin Networks. Current biology : CB *25*. https://doi.org/10.1016/j.cub.2015.04.038.

101. Blanchoin, L., Pollard, T.D., and Hitchcock-DeGregori, S.E. (2001). Inhibition of the Arp2/3 complex-nucleated actin polymerization and branch formation by tropomyosin. Current Biology *11*, 1300–1304. https://doi.org/10.1016/S0960-9822(01)00395-5.

102. Sikorski, R.S., and Hieter, P. (1989). A system of shuttle vectors and yeast host strains designed for efficient manipulation of DNA in Saccharomyces cerevisiae. Genetics *122*, 19–27. https://doi.org/10.1093/genetics/122.1.19.

103. Janke, C., Magiera, M.M., Rathfelder, N., Taxis, C., Reber, S., Maekawa, H., Moreno-Borchart, A., Doenges, G., Schwob, E., Schiebel, E., et al. (2004). A versatile toolbox for PCR-based tagging of yeast genes: new fluorescent proteins, more markers and promoter substitution cassettes. Yeast *21*, 947–962. https://doi.org/10.1002/yea.1142.

104. McInally, S.G., Kondev, J., and Goode, B.L. (2022). Quantitative Analysis of Actin Cable Length in Yeast. Bio Protoc *12*, e4402. https://doi.org/10.21769/BioProtoc.4402.

105. Collart, M.A., and Oliviero, S. (1993). Preparation of Yeast RNA. Current Protocols in Molecular Biology *23*, 13.12.1-13.12.5. https://doi.org/10.1002/0471142727.mb1312s23.

106. Schindelin, J., Arganda-Carreras, I., Frise, E., Kaynig, V., Longair, M., Pietzsch, T., Preibisch, S., Rueden, C., Saalfeld, S., Schmid, B., et al. (2012). Fiji: an open-source platform for biological-image analysis. Nat Methods *9*, 676–682. https://doi.org/10.1038/nmeth.2019.

107. Christianson, T.W., Sikorski, R.S., Dante, M., Shero, J.H., and Hieter, P. (1992). Multifunctional yeast high-copy-number shuttle vectors. Gene *110*, 119–122. https://doi.org/10.1016/0378-1119(92)90454-w.

108. Janke, C., Magiera, M.M., Rathfelder, N., Taxis, C., Reber, S., Maekawa, H., Moreno-Borchart, A., Doenges, G., Schwob, E., Schiebel, E., et al. (2004). A versatile toolbox for PCR-based tagging of yeast genes: new fluorescent proteins, more markers and promoter substitution cassettes. Yeast *21*, 947–962. https://doi.org/10.1002/yea.1142.

109. Pereira, G., and Schiebel, E. (2001). The role of the yeast spindle pole body and the mammalian centrosome in regulating late mitotic events. Current Opinion in Cell Biology *13*, 762–769. https://doi.org/10.1016/S0955-0674(00)00281-7.

970

971

Main Figure Legends

Figure 1: mNeonGreen-Tpm fusion proteins are functional and restore normal growth and actin cytoskeleton organization *in vivo*. (A) Representative time-lapse montages of wildtype yeast cells expressing mNG-^{AS}Tpm1 (top) or mNG-^{AS}Tpm2 (bottom); scale bar - 3μm. **(B)** Representative images of cells of indicated yeast strains stained with Rhodamine-phalloidin; scale bar - 3μm. **(C)** Plot representing mean actin cable length per cell for indicated strains as per experiment shown in (B). **(D)** Plot representing mean mitochondrial fragment count per cell for indicated strains as per experiment shown in S1G.
(Box represents 25th and 75th percentile, line represents median, whiskers represent minimum and maximum values; One-Way Anova with Tukey's Multiple Comparisons test was used in (C) and (D), * $p < 0.05$, ** $p < 0.01$, *** $p < 0.001$, **** $p < 0.0001$)

Figure 2: Tpm1 and Tpm2 colocalize and indiscriminately bind to actin filaments nucleated by formin isoforms, Bnr1 and Bni1. (A) Representative images of cells of wildtype, Δ*bnr1*, and Δ*bni1* cells expressing mNG-^{AS}Tpm1 fusion protein; scale bar - 3μm. **(B)** Superplot representing mean Tpm-bound cable length per cell in wildtype, Δ*bnr1*, and Δ*bni1* cells expressing mNG-^{AS}Tpm1; n=100 cells for each strain per replicate, N=3. **(C)** Superplot representing mean Tpm-bound cable number per cell in wildtype, Δ*bnr1*, and Δ*bni1* cells expressing mNG-^{AS}Tpm1; n=100 cells for each strain per replicate, N=3. **(D)** Representative images of cells of wildtype, Δ*bnr1*, and Δ*bni1* cells expressing mNG-^{AS}Tpm2 fusion protein; scale bar - 3μm. **(E)** Superplot representing mean Tpm-bound cable length per cell in wildtype, Δ*bnr1*, and Δ*bni1* cells expressing mNG-^{AS}Tpm2; n=100 cells for each strain per replicate, N=3. **(F)** Superplot representing mean Tpm-bound cable number per cell in wildtype, Δ*bnr1*, and Δ*bni1* cells expressing mNG-^{AS}Tpm2; n=100 cells for each strain per replicate, N=3. **(G)** Representative images of wildtype yeast cells co-expressing ymScarleti-^{AS}Tpm1 and mNG-^{AS}Tpm2; scale bar - 3μm.
(Superplots represent datapoints and means from three independent biological replicates marked in different colours; * $p < 0.05$, ** $p < 0.01$; One-Way Anova with Tukey's Multiple Comparisons test was used in (B), (C), (E), (F); * $p < 0.05$, ** $p < 0.01$)

Figure 3: Tpm1 and Tpm2 co-localize at the fusion focus in mating yeast cells in a Bni1-dependent manner. (A) Representative time-lapse montages of haploid *MATa* type wildtype yeast cell expressing mNG-^{AS}Tpm1 (left panel) or mNG-^{AS}Tpm2 (right panel) mating with haploid *MATα* wildtype yeast cell; scale bar – 2μm. **(B)** Representative time-lapse montages of haploid *MATa* type Δ*bnr1* yeast cell expressing mNG-^{AS}Tpm1 (left panel) or mNG-^{AS}Tpm2 (right panel) mating with haploid *MATα* wildtype yeast cell; scale bar – 2μm. **(C-D)** Line plot showing protein accumulation kinetics of

1007 mNG-^{AS}Tpm1 or mNG-^{AS}Tpm2 at the mating projection tip in wildtype (C) or Δ*bnr1* (D) cells. t=0 rep-
1008 resents cell fusion (n=3 fusion events/strain).
1009
1010 **Figure 4: Tpm2 can protect actin filaments from cofilin-mediated severing *in vitro*. (A)** Repre-
1011 sentative time-lapse images of the actin filaments before (left) and 2 min after the addition of recom-
1012 binant ScCofilin (right) in absence or presence of different Tpm isoforms; scale bar - 10µm. **(B)** Plot
1013 representing number of severing events per µm of actin filaments per minute. Data shown for inde-
1014 pendent trials; n≥150 filaments in each condition, N=3. **(C)** Plot representing actin filament lengths
1015 after 2 minutes of addition of Cof1 to the samples in absence (control) or presence of specified tropo-
1016 myosin; n= ~200 filaments, N=3.
1017 (Box represents 25th and 75th percentile, line represents median, whiskers represent minimum and
1018 maximum value; One-Way Anova with Tukey's Multiple Comparisons test was used in (B) and (C) *
1019 p < 0.05, ** p < 0.01, *** p < 0.001, **** p < 0.0001)
1020
1021 **Figure 5: Increased Tpm2 expression can restore actin cables in Δ*tpm1* cells. (A)** Representa-
1022 tive images of indicated yeast strains stained with Alexa488-phalloidin; scale bar – 3µm. **(B)** Plot
1023 representing mean percentage of cells with detectable actin cables in indicated yeast strains aver-
1024 aged over 3 biological replicates; n>150 cells for each strain per replicate, N=3. **(C)** Plot representing
1025 mean actin cable length per cell in the indicated yeast strains as per experiment in (A); n=50 cells for
1026 each strain. **(D)** Representative time-course images of wildtype and Δ*tpm2* cells treated with Latrun-
1027 culin B (67µM) and stained with Alexa488-phalloidin; scale bar - 2µm. **(E)** Plot representing mean
1028 percentage of cells with detectable actin cables in indicated yeast strains averaged over 3 biological
1029 replicates; n>125 cells per strain per replicate, N=3.
1030 (Box represents 25th and 75th percentile, line represents median, whiskers represent minimum and
1031 maximum value; One-Way Anova with Tukey's Multiple Comparisons test was used in (C) and Un-
1032 paired two-tailed t-test was used in (E), * p < 0.05, ** p < 0.01, *** p < 0.001, **** p < 0.0001)
1033
1034 **Figure 6: Tpm2 can independently organize a functional actin cytoskeleton in *Δtpm1* cells and**
1035 **(A)** Representative images of indicated yeast strains expressing ymScarleti-Sec4; scale bar – 3µm.
1036 **(B)** Representative images of indicated yeast strains expressing Su9-mNeonGreen; Scale bar – 3µm.
1037 **(C)** Plot representing ratio of bud/mother ymScarleti-Sec4 fluorescence per cell in the indicated yeast
1038 strains; n≥25 cells per strain. **(D)** Plot representing mean mitochondrial fragment count per cell in the
1039 indicated yeast strains; n≥30 cells per strain. **(E)** Representative time-lapse images of actin patch
1040 dynamics in cells with indicated genotypes expressing LifeAct-eGFP, scale bar – 0.65µm. **(F)** Box
1041 and Whiskers plot showing actin patch lifetimes in the indicates yeast strains, (n>20 patches/strain).

1042 **(G)** Box and Whiskers plot showing mean LifeAct-eGFP fluorescence in the indicates yeast strains,
1043 ($n \geq 735$ cells/strain).
1044 (Box represents 25th and 75th percentile, line represents median, whiskers represent minimum and
1045 maximum value; One-Way Anova with Tukey's Multiple Comparisons test was used in (C), Kruskal-
1046 Wallis test with Dunn's multiple comparisons test was used in (D), (G), and (F); * $p < 0.05$, ** $p < 0.01$
1047 * $p < 0.05$, ** $p < 0.01$, *** $p < 0.001$, **** $p < 0.0001$)
1048

1049 **Supplementary Figure Legends**

1050

1051 **Figure S1: Functional characterization of mNeonGreen-Tpm fusion proteins**. **(A)** Representative
1052 time-lapse montages of wildtype yeast cells expressing mNG-Tpm1; scale bar - 3μm. **(B)** Representa-
1053 tive time-lapse montages of wildtype yeast cells expressing mNG-Tpm2; scale bar - 3μm. **(C)** Plot
1054 representing growth curves of indicated yeast strains performed at 37°C. y-axis represents mean
1055 absorbance at 600nm. **(D)** Spot assay image for indicated yeast strains performed at 23°C, 30°C, and
1056 37°C. **(E)** Representative images of cells of indicated yeast strains stained with Rhodamine-phalloidin;
1057 scale bar – 2μm. **(F)** Representative images of cells expressing indicated mNeonGreen-Tpm fusion
1058 proteins stained with Rhodamine-phalloidin; scale bar - 2μm. **(G)** Representative images of indicated
1059 yeast strains expressing Om45-3xmCherry from the native locus; scale bar - 2μm.

1060

1061 **Figure S2: Tpm1 and Tpm2 bind to actin filaments made by formins Bnr1 and Bni1 indiscrim-**
1062 **inately. (A)** Representative images of cells of wildtype, Δ*bnr1*, and Δ*bni1* cells expressing mNG-
1063 ^{AS}Tpm1 stained with Rhodamine-phalloidin; scale bar - 2μm. **(B)** Superplot representing mean actin
1064 cable length per cell in wildtype, Δ*bnr1*, and Δ*bni1* cells expressing mNG-^{AS}Tpm1; n=100 cells per
1065 strain per replicate, N=3. **(C)** Superplot representing mean actin cable number per cell in wildtype,
1066 Δ*bnr1*, and Δ*bni1* cells expressing mNG-^{AS}Tpm1; n=100 per strain per replicate, N=3. **(D)** Repre-
1067 sentative images of cells of wildtype, Δ*bnr1*, and Δ*bni1* cells expressing mNG-^{AS}Tpm2 stained with
1068 Rhodamine-phalloidin; scale bar – 2μm. **(E)** Superplot representing mean actin cable length per cell
1069 in wildtype, Δ*bnr1*, and Δ*bni1* cells expressing mNG-^{AS}Tpm2; n=100 cells per strain per replicate,
1070 N=3. **(F)** Superplot representing mean actin cable number per cell in wildtype, Δ*bnr1*, and Δ*bni1* cells
1071 expressing mNG-^{AS}Tpm2; n=100 cells per strain per replicate, N=3. **(G)** Box and whiskers plot show-
1072 ing ratio of mean mNG fluorescence in the bud to the mother compartment in the indicated strains.
1073 Box represents 25th and 75th percentile, line represents median, whiskers represent minimum and
1074 maximum value.
1075 (Superplots represent datapoints and means from three independent biological replicates marked in
1076 different colours; One-Way Anova with Tukey's Multiple Comparisons test was used in (B), (C), (E),
1077 (F); * $p < 0.05$, ** $p < 0.01$)

1078

1079 **Figure S3: mNG-^{AS}Tpm1 shows binding to both Bnr1- and Bni1-made cables even in the ab-**
1080 **sence of endogenous Tpm1. (A)** Representative images of Δ*tpm1* cells expressing mNG-^{AS}Tpm1
1081 fusion protein as sole copy with indicated genotypes; scale bar - 2μm. **(B)** Superplot representing
1082 mean Tpm-bound cable length per cell in indicated strains expressing mNG-^{AS}Tpm1 as sole copy;
1083 n=25 cells per strain per replicate, N=3. **(C)** Superplot representing mean Tpm-bound cable number

per cell in indicated strains expressing mNG-^{AS}Tpm1 as a sole copy; n=25 cells per strain per replicate, N=3. **(D)** Representative images of Δ*tpm1* cells expressing mNG-^{AS}Tpm1 fusion protein as sole copy with indicated genotypes stained with Rhodamine-phalloidin; scale bar - 2μm. **(E)** Superplot representing mean actin cable length per cell in indicated yeast strains shown in (D); n=15 cells per strain per replicate, N=3. **(F)** Superplot representing mean actin cable number per cell in in indicated yeast strains shown in (D); n=15 per strain per replicate, N=3.
(Superplots represent datapoints and means from three independent biological replicates marked in different colours; One-Way Anova with Tukey's Multiple Comparisons test was used in (B), (C), (E), (F); * $p < 0.05$, ** $p < 0.01$, *** $p < 0.001$, **** $p < 0.0001$)

Figure S4: Tpm2 overexpression restores actin cables in *Δtpm1* cells. (A) Spot assay image for indicated yeast strains performed at 23°C, 30°C, and 37°C. **(B)** Representative images of indicated yeast strains stained with Alexa488-phalloidin; scale bar – 2μm. **(C)** Plot representing mean percentage of cells with detectable actin cables in indicated yeast strains averaged over 3 biological replicates; n≥200 cells for each strain per replicate, N=3. **(D)** Plot representing fold change of Tpm2 transcript levels normalized to wildtype in the indicated yeast strains; n=3 per strain per experiment, N=3. **(E)** Plot representing fold change of Tpm2 transcript levels normalized to *wildtype* in the indicated yeast strains; n=3 per strain per experiment, N=3. **(F)** Spot assay image for indicated yeast strains performed at 23°C, 30°C, and 37°C.
(Box represents 25th and 75th percentile, line represents median, whiskers represent minimum and maximum value; One-Way Anova with Tukey's Multiple Comparisons test was used in (C), (D) and (E).s * $p < 0.05$, ** $p < 0.01$, *** $p < 0.001$, **** $p < 0.0001$)

Figure S5: Increased protein levels of mNG-^{AS}Tpm2 cause a rescue of phenotype in *Δtpm1* cells. (A) Spot Assay showing growth of indicated yeast strains at 23°C, 30°C, and 37°C. **(B)** Representative images of yeast cells with indicated genotypes, scale bar - 2μm. **(C)** Plot showing mean mNG fluorescence intensity per cell in the indicated yeast strains, n>174 cells per strain. **(D)** Representative image of western blot probed with anti-mNG and anti-actin (loading control). **(E)** Plot showing normalized fold change of mNG/actin signal intensity for blot shown in (D), N=3.
(One-Way Anova with Tukey's Multiple Comparisons test was used in (C) and (E). * $p < 0.05$, ** $p < 0.01$, *** $p < 0.001$, **** $p < 0.0001$)

Figure S6: Tpm2 overexpression restores actin cable dependent functions in *Δtpm1* cells. (A) Representative images of indicated yeast strains expressing ymScarleti-Sec4; scale bar – 2μm. **(B)** Representative images of indicated yeast strains expressing Su9-mNeonGreen; scale bar – 2μm. **(C)** Plot representing ratio of bud/mother ymScarleti-Sec4 fluorescence per cell in the indicated yeast

1120 strains; n≥24 cells per strain. **(D)** Plot representing mean mitochondrial fragment count per cell in the
1121 indicated yeast strains; n≥25 cells per strain. **(E)** Representative time-lapse montages of wildtype
1122 yeast cells expressing LifeAct-eGFP from its native locus, scale bar - 2μm. **(F)** Plot representing ret-
1123 rograde actin cable flow rate (μm/s) in the indicated yeast strains; n≥20 events per strain.
1124 (Box represents 25th and 75th percentile, line represents median, whiskers represent minimum and
1125 maximum value; One-Way Anova with Tukey's Multiple Comparisons test was used in (C), (F); Krus-
1126 kal-Wallis test with Dunn's multiple comparisons was used in (D); * $p < 0.05$, ** $p < 0.01$, *** $p < 0.001$,
1127 **** $p < 0.0001$)
1128
1129 **Figure S7**: **Analysis piplelines used for quantitative analysis of actin cables and mitochondrial**
1130 **morphology in our study. (A)** Schematic showing quantification workflow for actin cables as
1131 adapted from *McInally et al. 2022* (*bio-protocol*). **(B)** Schematic showing quantification workflow for
1132 mitochondrial morphology analysis using Mitochondria Analyzer Plug-In in Fiji.
1133
1134 **Supplementary Movie 1**. Time-lapse imaging of small-, medium- and large-budded cells expressing
1135 mNeonGreen-^{AS}Tpm1. (Scale bar - 3μm)
1136
1137 **Supplementary Movie 2**. Time-lapse imaging of small-, medium- and large-budded cells expressing
1138 mNeonGreen-^{AS}Tpm2. (Scale bar - 3μm)
1139
1140 **Supplementary Movie 2**. Time-lapse imaging of haploid yeast cell expressing mNeonGreen-^{AS}Tpm1
1141 mating with another wildtype haploid cell. (Scale bar - 3μm)
1142
1143 **Supplementary Movie 2**. Time-lapse imaging of haploid yeast cell expressing mNeonGreen-^{AS}Tpm2
1144 mating with another wildtype haploid cell. (Scale bar - 3μm)
1145

1146 **Supplementary Table 1. List of plasmids used in this study.**

1147

Plasmid Number	Description	Source
piSP1	*pRS305*	*Sikorski and Hieter, 1989*[102]
piSP5	*pRS315*	*Sikorski and Hieter, 1989*[102]
piSP6	*pRS316*	*Sikorski and Hieter, 1989*[102]
piSP11	*pRS425*	*Christianson et al. 1992*[107]
piSP14	*pYM25 (yeGFP-hphNT2)*	*Janke et al. 2004*[108]
piSP346	*pRS305-pTpm1-mNG-40L-Tpm1-tCYC*	This Study
piSP348	*pRS305-pTpm2-mNG-40L-Tpm2-tCYC*	This Study
piSP1422	*pRS305-pTpm1-mNG-40L-^{AS}Tpm1-tTpm1*	This Study
piSP1423	*pRS305-pTpm2-mNG-40L-^{AS}Tpm2-tTpm2*	This Study
piSP1430	*pRS316-pTpm1-TPM1-tTpm1*	This Study
piSP1493	*pRS425-pTpm2-TPM2-tTpm2*	This Study
piSP1450	*pRS316-pTpm1-TPM2-tTpm2*	This Study
piSP1451	*pRS306-pADH-ymScarlet-Sec4*	This Study
piSP1529	*pRS316-pTpm2-TPM2-tTpm2*	This Study
piSP1534	*pET28a-6His-Cof1*	This Study
piSP1541	*pRS316-pTpm2-TPM1-tTpm1*	This Study
piSP1644	*pETMCN-^{AS}Tpm1*	This Study
piSP1646	*pETMCN-^{AS}Tpm2*	This Study
piSP1825	*pRS305-pADH-ymScarlet-Sec4-tCYC*	This Study
piSP1826	*pRS315-pTpm1-TPM2-tTpm2*	This Study
piSP1827	*pRS315-pTpm2-TPM1-tTpm1*	This Study
piSP1828	*pRS315-pTpm2-TPM2-tTpm2*	This Study
piSP1829	*pRS305-pCYC-Su9-mNG-tCYC*	This Study
piSP1830	*pRS306-pCYC-Su9-mNG-tCYC*	This Study
piSP1831	*pRS315-pTpm1-TPM1-tTpm1*	This Study
piSP1836	*pRS306-pTpm1-ymScarleti-40L-^{AS}Tpm1-tTpm1*	This Study
piSP2034	*pRS305-pADH-LifeAct-eGFP-tCYC*	This Study

1148

1149

1150

1151

1152

1153

1154 **Supplementary Table 2. List of yeast strains used in this study.**

1155

Strain Number	Genotype	Source
YSP002	*MATa ura3-52 leu2Δ1 trp1Δ63 his3Δ200*	*Pereira and Schiebel*, 2001[109]
YSP003	*MATα ura3-52 lys2-801amber ade2-101ochre trp1Δ63 his3Δ200 leu2Δ1*	*Sikorski and Hieter*, 1989[102]
YSP107	*MATa ura3-52 leu2Δ1 trp1Δ63 his3Δ200 pRS305-pTpm1-mNG-40aaL-Tpm1-tTpm1*	This study
YSP108	*MATa ura3-52 leu2Δ1 trp1Δ63 his3Δ200 pRS305-pTpm2-mNG-40aaL-Tpm2-tTpm2*	This study
YSP146	*MATa ura3-52 leu2Δ1 trp1Δ63 his3Δ200 -Δtpm1-HIS3MX6-pRS305-pTpm1-mNG-40L-Tpm1-tTpm1*	This study
YSP195	*MATa ura3-52 leu2Δ1 trp1Δ63 his3Δ200-Δtpm1-HIS3MX6*	
YSP196	*MATa ura3-52 leu2Δ1 trp1Δ63 his3Δ200-Δtpm2-HIS3MX6*	
YSP227	*MATa ura3-52 leu2Δ1 trp1Δ63 his3Δ200 -Δtpm1-HIS3MX6-pRS305*	This study
YSP355	*MATa ura3-52 leu2Δ1 trp1Δ63 his3Δ200 -pRS305-pTpm1-mNG-40aaL-(AM)Tpm1-tTpm1*	This study
YSP356	*MATa ura3-52 leu2Δ1 trp1Δ63 his3Δ200 -pRS305-pTpm2-mNG-40aaL-(am)Tpm2-tTpm2*	This study
YSP419	*MATa ura3-52 leu2Δ1 trp1Δ63 his3Δ200 -Δtpm1-HIS3MX6-pRS305-pTpm1-mNG-40L-^{AS}Tpm1-tTpm1*	This study
YSP440	*MATa ura3-52 leu2Δ1 trp1Δ63 his3Δ200 -pRS305-pTpm1-mNG-40aaL-(am)Tpm1-tTpm1 -Δbnr1-HIS3MX6*	This study
YSP441	*MATa ura3-52 leu2Δ1 trp1Δ63 his3Δ200 -pRS305-pTpm2-mNG-40aaL-(am)Tpm2-tTpm2-Δbnr1-HIS3MX6*	This study
YSP442	*MATa ura3-52 leu2Δ1 trp1Δ63 his3Δ200 -pRS305-pTpm2-mNG-40aaL-Tpm2-tTp-Δbni1-HIS3MX6*	This study
YSP443	*MATa ura3-52 leu2Δ1 trp1Δ63 his3Δ200 -pRS305-pTpm1-mNG-40aaL-(am)Tpm1-tTpm1 -Δbni1-HIS3MX6*	This study

YSP609	*MATa ura3-52 leu2Δ1 trp1Δ63 his3Δ200 -Δtpm1-HIS3MX6-pRS305-pTpm1-mNG-40L-Tpm1-tTpm1 - OM45-3XmCherry-Kan*	This study
YSP610	*MATa ura3-52 leu2Δ1 trp1Δ63 his3Δ200 -Δtpm1-HIS3MX6-OM45-3XmCherry-Kan*	This study
YSP611	*MATa ura3-52 leu2Δ1 trp1Δ63 his3Δ200 -Δtpm1-HIS3MX6-pRS305-pTpm1-mNG-40L-^{AS}Tpm1-tTpm1 -OM45-3XmCherry-Kan*	This study
YSP612	*MATa ura3-52 leu2Δ1 trp1Δ63 his3Δ200 --OM45-3XmCherry-Kan*	This study
YSP671	*MATa ura3-52 leu2Δ1 trp1Δ63 his3Δ200 -pRS305-pTpm2-mNG-40aaL-(AM)Tpm2-tTpm2 - pRS306-pTpm1-ymScarletiI-40aaLinker-(AM)Tpm1-tTpm1*	This study
YSP685	*MATa ura3-52 leu2Δ1 trp1Δ63 his3Δ200 - Δtpm1-HIS3MX6-pRS425*	This study
YSP686	*MATa ura3-52 leu2Δ1 trp1Δ63 his3Δ200 -Δtpm1-HIS3MX6-pRS425-pTpm2-Tpm2-tTpm2*	This study
YSP767	*MATa ura3-52 leu2Δ1 trp1Δ63 his3Δ200 -Δtpm1-HIS3MX6 -pRS425-pTpm2-mNG-40L-^{AS}Tpm2-tTpm2*	This study
YSP780	*MATa ura3-52 leu2Δ1 trp1Δ63 his3Δ200 -Δtpm1-his3MX6-pRS305-pTpm1-mNG-40L-^{AS}Tpm1-tTpm1 - Δbnr1-hphNT1*	This study
YSP794	*MATa ura3-52 leu2Δ1 trp1Δ63 his3Δ200 -Δtpm1-HIS3MX6 -pRS425-pTpm1-mNG-40L-^{AS}Tpm1-tTpm1*	This study
YSP824	*MATa ura3-52 leu2Δ1 trp1Δ63 his3Δ200 -Δtpm1-HIS3MX6 -pRS306-pADH-ymScarleti-Sec4*	This study
YSP835	*MATa ura3-52 leu2Δ1 trp1Δ63 his3Δ200 - pRS425 - pRS316*	This study
YSP836	*MATa ura3-52 leu2Δ1 trp1Δ63 his3Δ200 - pRS306-pADH-ymScarleti-Sec4*	This study
YSP837	*MATa ura3-52 leu2Δ1 trp1Δ63 his3Δ200 -Δtpm1-HIS3MX6-pRS425-pTpm2-Tpm2-tTpm2 - pRS306-pADH-ymScarleti-Sec4*	This study
YSP848	*MATa ura3-52 leu2Δ1 trp1Δ63 his3Δ200 -Δtpm1-HIS3MX6 -pRS316-pTpm2-Tpm1-tTpm1*	This study
YSP887	*MATa ura3-52 leu2Δ1 trp1Δ63 his3Δ200 -Δtpm1-HIS3MX6 -pRS316*	This study

YSP907	*MATa ura3-52 leu2Δ1 trp1Δ63 his3Δ200Δtpm1-HIS3MX6; pRS316-pTpm1-Tpm1-tTpm1*	This study
YSP909	*MATa ura3-52 leu2Δ1 trp1Δ63 his3Δ200Δtpm1-HIS3MX6; pRS316-pTpm2-Tpm2-tTpm2*	This study
YSP1090	*MATa ura3-52 leu2Δ1 trp1Δ63 his3Δ200-Δtpm1-HIS3MX6; pRS316-pTpm1-Tpm2-tTpm2*	This study
YSP1117	*MATa ura3-52 leu2Δ1 trp1Δ63 his3Δ200-pRS306-pCYC-Su9-mNG-tCYC - pRS425*	This study
YSP1118	*MATa ura3-52 leu2Δ1 trp1Δ63 his3Δ200-Δtpm1-HIS3MX6-pRS425 - pRS306-pCYC-Su9-mNG-tCYC*	This study
YSP1119	*MATa ura3-52 leu2Δ1 trp1Δ63 his3Δ200-Δtpm1-HIS3MX6-pRS425-pTpm2-Tpm2-tTpm2 - pRS306-pCYC-Su9-mNG-tCYC*	This study
YSP1120	*MATa ura3-52 leu2Δ1 trp1Δ63 his3Δ200-Δtpm1-HIS3MX6 - pRS306-pADH-ymScarleti-Sec4 - pRS315*	This study
YSP1121	*MATa ura3-52 leu2Δ1 trp1Δ63 his3Δ200-Δtpm1-HIS3MX6 - pRS306-pADH-ymScarleti-Sec4 - pRS315-pTpm1-Tpm2-tTpm2*	This study
YSP1122	*MATa ura3-52 leu2Δ1 trp1Δ63 his3Δ200-Δtpm1-HIS3MX6 - pRS306-pADH-ymScarleti-Sec4 - pRS315-pTpm2-Tpm1-tTpm1*	This study
YSP1123	*MATa ura3-52 leu2Δ1 trp1Δ63 his3Δ200-Δtpm1-HIS3MX6 - pRS306-pADH-ymScarleti-Sec4 - pRS315-pTpm2-Tpm2-tTpm2*	This study
YSP1126	*MATa ura3-52 leu2Δ1 trp1Δ63 his3Δ200 pRS305-pCYC-Su9-mNG-tCYC pRS216*	This study
YSP1127	*MATa ura3-52 leu2Δ1 trp1Δ63 his3Δ200 Δtpm1-HIS3MX6 - pRS305-pCYC-Su9-mNG-tCYC*	This study
YSP1128	*MATa ura3-52 leu2Δ1 trp1Δ63 his3Δ200 Δtpm1-HIS3MX6 - pRS316-pTpm2-Tpm1-tTpm1 - pRS305-pCYC-Su9-mNG-tCYC*	This study
YSP1129	*MATa ura3-52 leu2Δ1 trp1Δ63 his3Δ200 Δtpm1-HIS3MX6; pRS316-pTpm1-Tpm1-tTpm1- pRS305-pCYC-Su9-mNG-tCYC*	This study

YSP1130	*MATa ura3-52 leu2Δ1 trp1Δ63 his3Δ200 Δtpm1-HIS3MX6; pRS316-pTpm2-Tpm2-tTpm2- pRS305-pCYC-Su9-mNG-tCYC*	This study
YSP1131	*MATa ura3-52 leu2Δ1 trp1Δ63 his3Δ200 Δtpm1-HIS3MX6; pRS316-pTpm1-Tpm2-tTpm2- pRS305-pCYC-Su9-mNG-tCYC*	This study
YSP1150	*MATa ura3-52 leu2Δ1 trp1Δ63 his3Δ200-Δtpm1-HIS3MX6 - pRS306-pADH-ymScarleti-Sec4 , pRS315-pTpm1-Tpm1-tTpm1*	This study
YSP1189	*MATa ura3-52 leu2Δ1 trp1Δ63 his3Δ200-Abp140-GFP-KanMX6*	This study
YSP1191	*MATa ura3-52 leu2Δ1 trp1Δ63 his3Δ200-Δtpm2-HIS3MX6 - Abp140-GFP-KanMX6*	This study
YSP1192	*MATa ura3-52 leu2Δ1 trp1Δ63 his3Δ200-Δtpm2-HIS3MX6) - pRS425-pTpm2-Tpm2-tTpm2) - Abp140-GFP-KanMX6*	This study
YSP1577	*MATa ura3-52 leu2Δ1 trp1Δ63 his3Δ200 Δtpm1-His3MX6-Δbni1-hph - pRS305-pTpm1-mNG-40L-^{AS}Tpm1-tTpm*	This study
YSP1639	*MATa ura3-52 leu2Δ1 trp1Δ63 his3Δ200 - Δtpm1-his3MX6 - pRS305-pTpm2-mNG-^{AS}Tpm2-tTpm2*	This study
YSP1816	*MATa ura3-52 leu2Δ1 trp1Δ63 his3Δ200 pRS305-pADH-Life-Act-eGFP-tCYC - Δtpm1::his3MX6 - pRS316 (empty)*	This study
YSP1817	*MATa ura3-52 leu2Δ1 trp1Δ63 his3Δ200 pRS305-pADH-Life-Act-eGFP-tCYC - Δtpm2::his3MX6 - pRS316 (empty)*	This study
YSP1818	*MATa ura3-52 leu2Δ1 trp1Δ63 his3Δ200 pRS305-pADH-Life-Act-eGFP-tCYC - pRS316 (empty)*	This study
YSP1819	*MATa ura3-52 leu2Δ1 trp1Δ63 his3Δ200 pRS305-pADH-Life-Act-eGFP-tCYC - Δtpm1::his3MX6 - pRS316-pTpm1-Tpm1-tTpm1 (GD13)*	This study
YSP1820	*MATa ura3-52 leu2Δ1 trp1Δ63 his3Δ200 pRS305-pADH-Life-Act-eGFP-tCYC - Δtpm2::his3MX6 - pRS316-pTpm1-Tpm1-tTpm1 (GD13)*	This study
YSP1822	*MATa ura3-52 leu2Δ1 trp1Δ63 his3Δ200 pRS305-pADH-Life-Act-eGFP-tCYC - Δtpm1::his3MX6 - pRS316-pTpm1-Tpm1-tTpm1 (GT34)*	This study

YSP1823	*MATa ura3-52 leu2Δ1 trp1Δ63 his3Δ200 pRS305-pADH-Life-Act-eGFP-tCYC - Δtpm2::his3MX6 - pRS316-pTpm1-Tpm1-tTpm1 (GT34)*	This study

1156

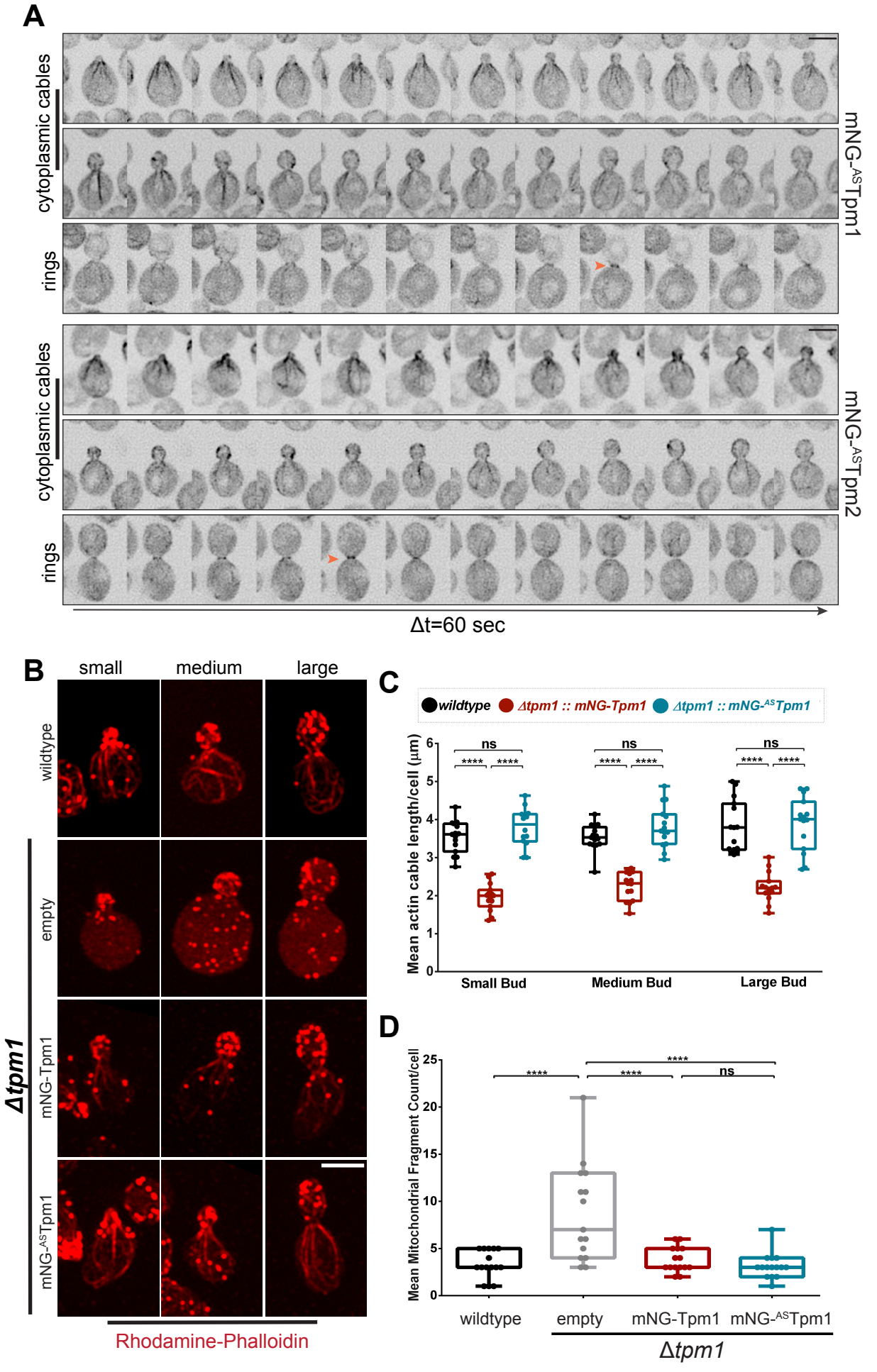
A
cytoplasmic cables
rings
mNG-ASTpm1
cytoplasmic cables
rings
mNG-ASTpm2
Δt=60 sec
B
small
medium
large
wildtype
empty
mNG-Tpm1
mNG-ASTpm1
Δtpm1
Rhodamine-Phalloidin
C
wildtype
Δtpm1 :: mNG-Tpm1
Δtpm1 :: mNG-ASTpm1
Mean actin cable length/cell (µm)
ns
****
Small Bud
Medium Bud
Large Bud
D
Mean Mitochondrial Fragment Count/cell
****
ns
wildtype
empty
mNG-Tpm1
mNG-ASTpm1
Δtpm1

Figure 2 Dhar et al

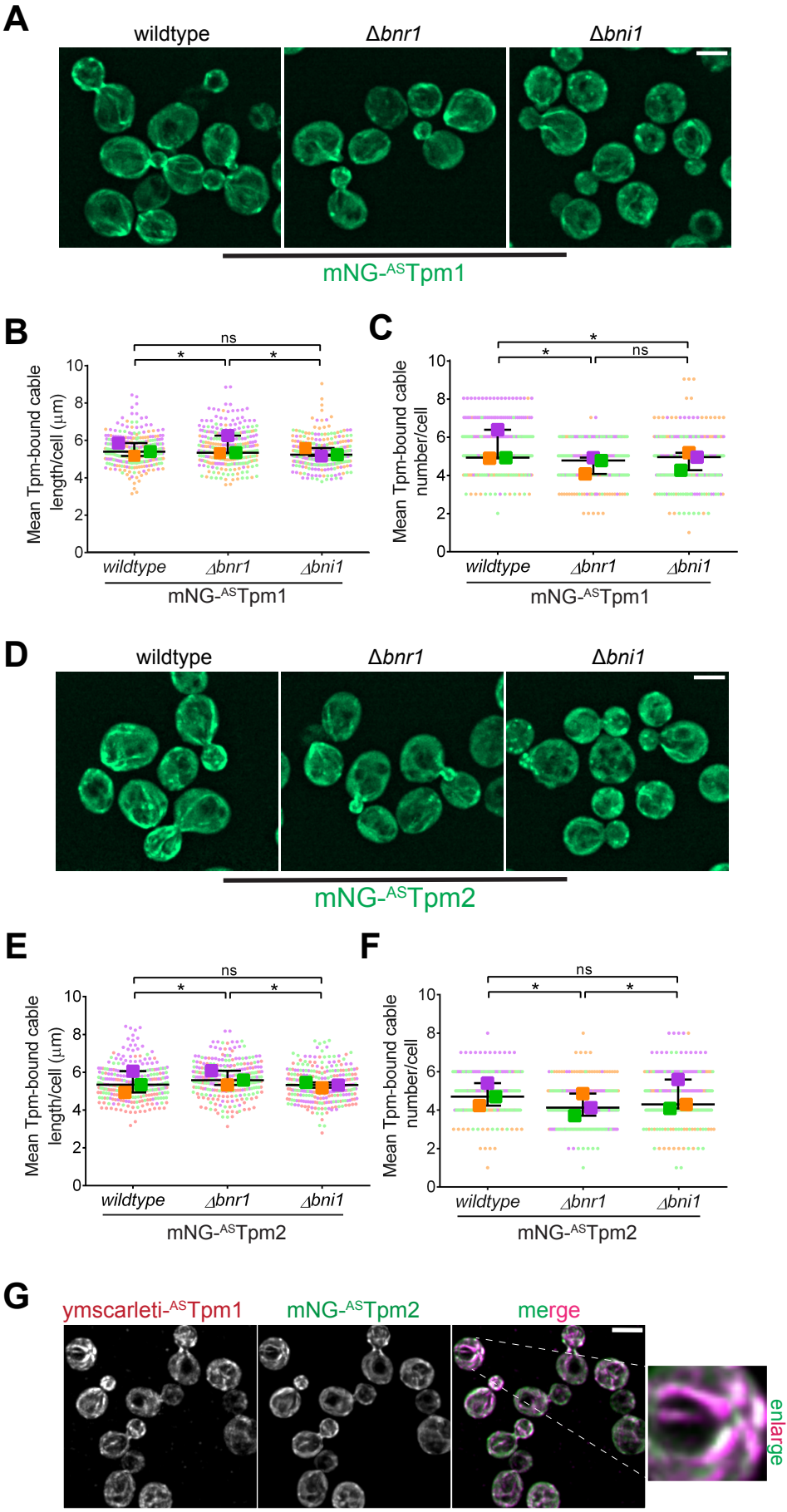

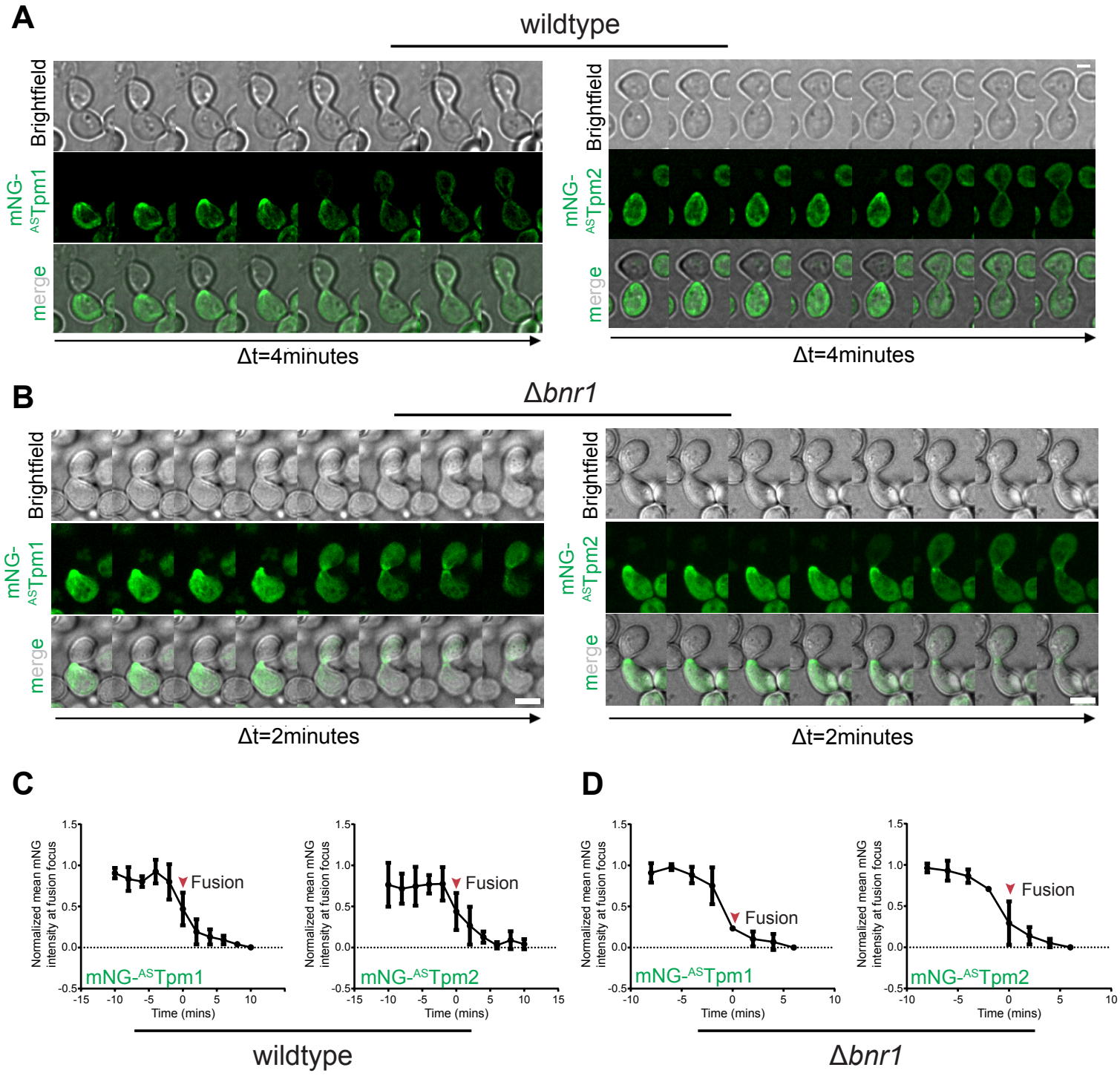
A
wildtype
Brightfield
mNG-ASTpm1
merge
Δt=4minutes
Brightfield
mNG-ASTpm2
merge
Δt=4minutes
B
Δbnr1
Brightfield
mNG-ASTpm1
merge
Δt=2minutes
Brightfield
mNG-ASTpm2
merge
Δt=2minutes
C
D
Normalized mean mNG intensity at fusion focus
Fusion
mNG-ASTpm1
mNG-ASTpm2
Time (mins)
wildtype
Δbnr1

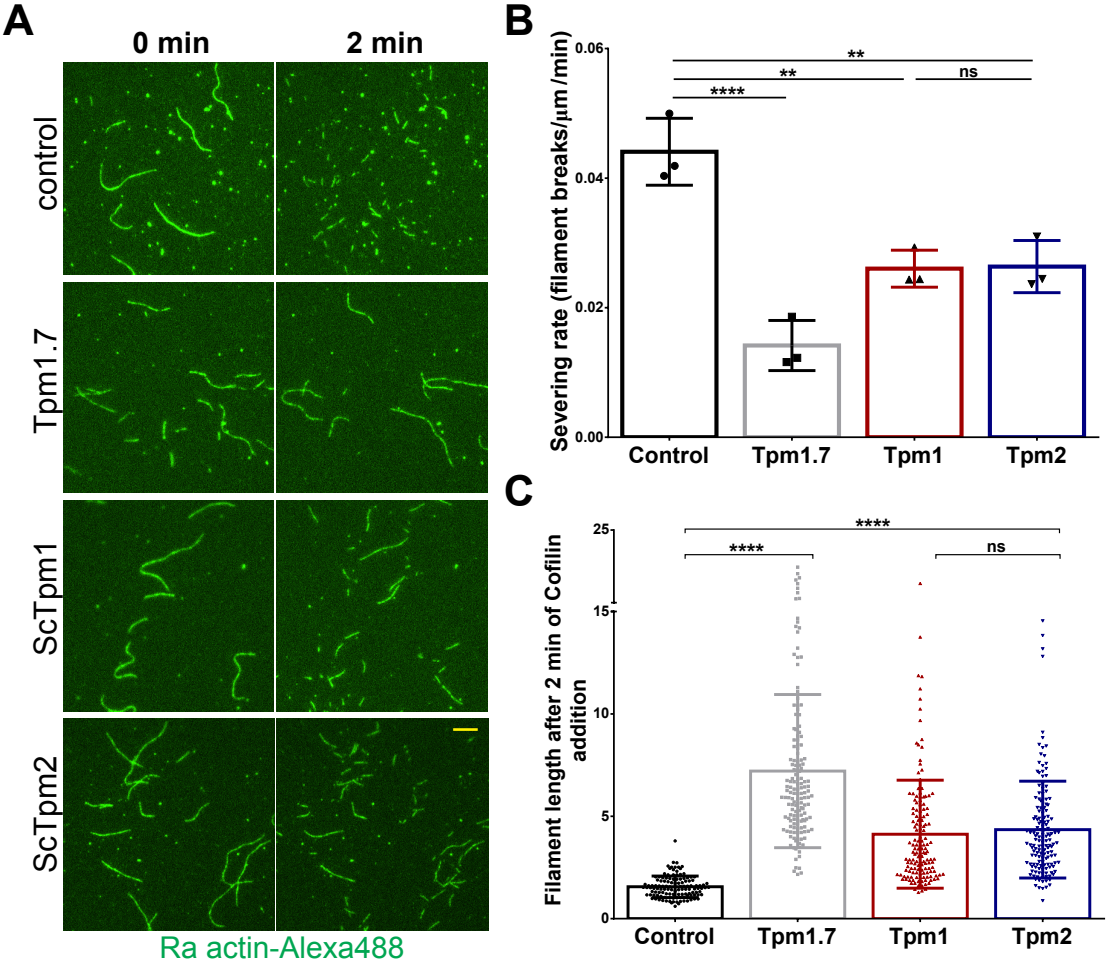
A
0 min
2 min
control
Tpm1.7
ScTpm1
ScTpm2
Ra actin-Alexa488
B
Severing rate (filament breaks/µm/min)
0.06
0.04
0.02
0.00
**
**
****
ns
Control
Tpm1.7
Tpm1
Tpm2
C
Filament length after 2 min of Cofilin addition
25
15
10
5
0
****
****
ns
Control
Tpm1.7
Tpm1
Tpm2

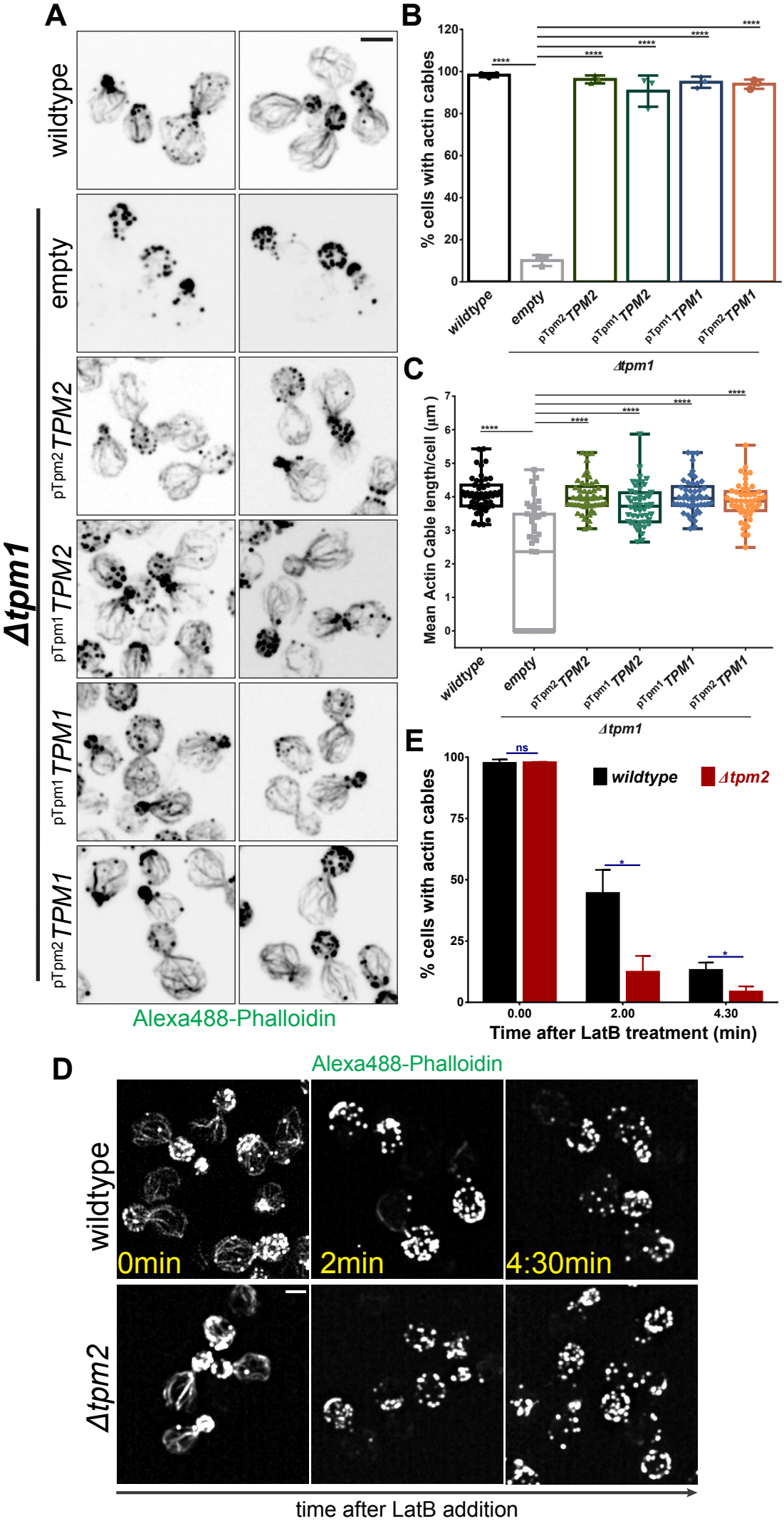
A
wildtype
empty
pTpm2 TPM2
pTpm1 TPM2
pTpm1 TPM1
pTpm2 TPM1
Δtpm1
Alexa488-Phalloidin
B
% cells with actin cables
wildtype
empty
pTpm2-TPM2
pTpm1 TPM2
pTpm1 TPM1
pTpm2-TPM1
Δtpm1
C
Mean Actin Cable length/cell (µm)
E
% cells with actin cables
wildtype
Δtpm2
ns
Time after LatB treatment (min)
D
Alexa488-Phalloidin
0min
2min
4:30min
time after LatB addition

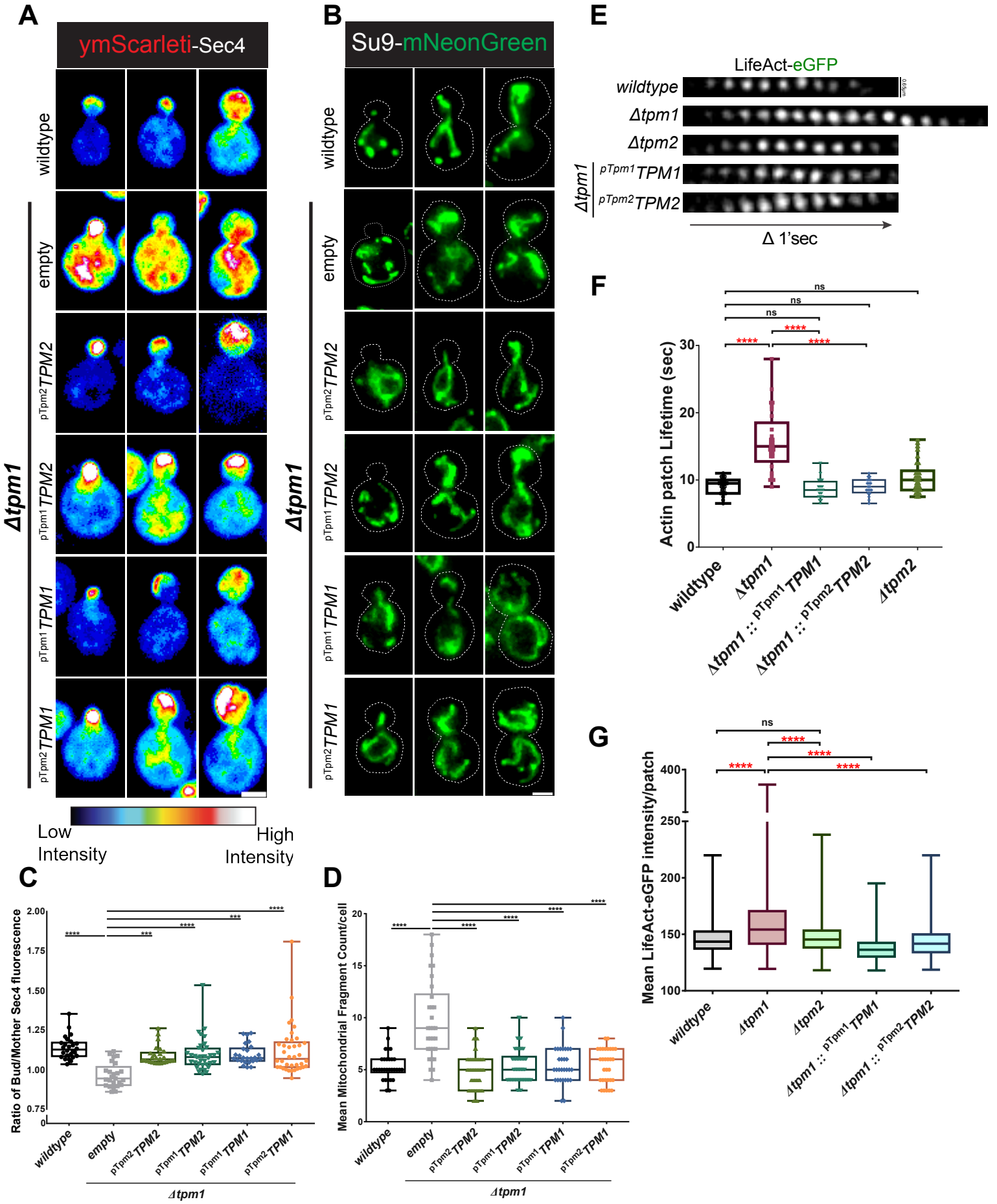
A
ymScarleti-Sec4
wildtype
empty
pTpm2TPM2
pTpm1TPM2
pTpm1TPM1
pTpm2TPM1
Δtpm1
Low Intensity
High Intensity
B
Su9-mNeonGreen
wildtype
empty
pTpm2TPM2
pTpm1TPM2
pTpm1TPM1
pTpm2TPM1
Δtpm1
C
Ratio of Bud/Mother Sec4 fluorescence
wildtype
empty
pTpm2TPM2
pTpm1TPM2
pTpm1TPM1
pTpm2TPM1
Δtpm1
D
Mean Mitochondrial Fragment Count/cell
wildtype
empty
pTpm2TPM2
pTpm1TPM2
pTpm1TPM1
pTpm2TPM1
Δtpm1
E
LifeAct-eGFP
wildtype
Δtpm1
Δtpm2
Δtpm1
pTpm1TPM1
pTpm2TPM2
Δ 1'sec
F
Actin patch Lifetime (sec)
wildtype
Δtpm1
Δtpm1 :: pTpm1TPM1
Δtpm1 :: pTpm2TPM2
Δtpm2
G
Mean LifeAct-eGFP intensity/patch
wildtype
Δtpm1
Δtpm2
Δtpm1 :: pTpm1TPM1
Δtpm1 :: pTpm2TPM2

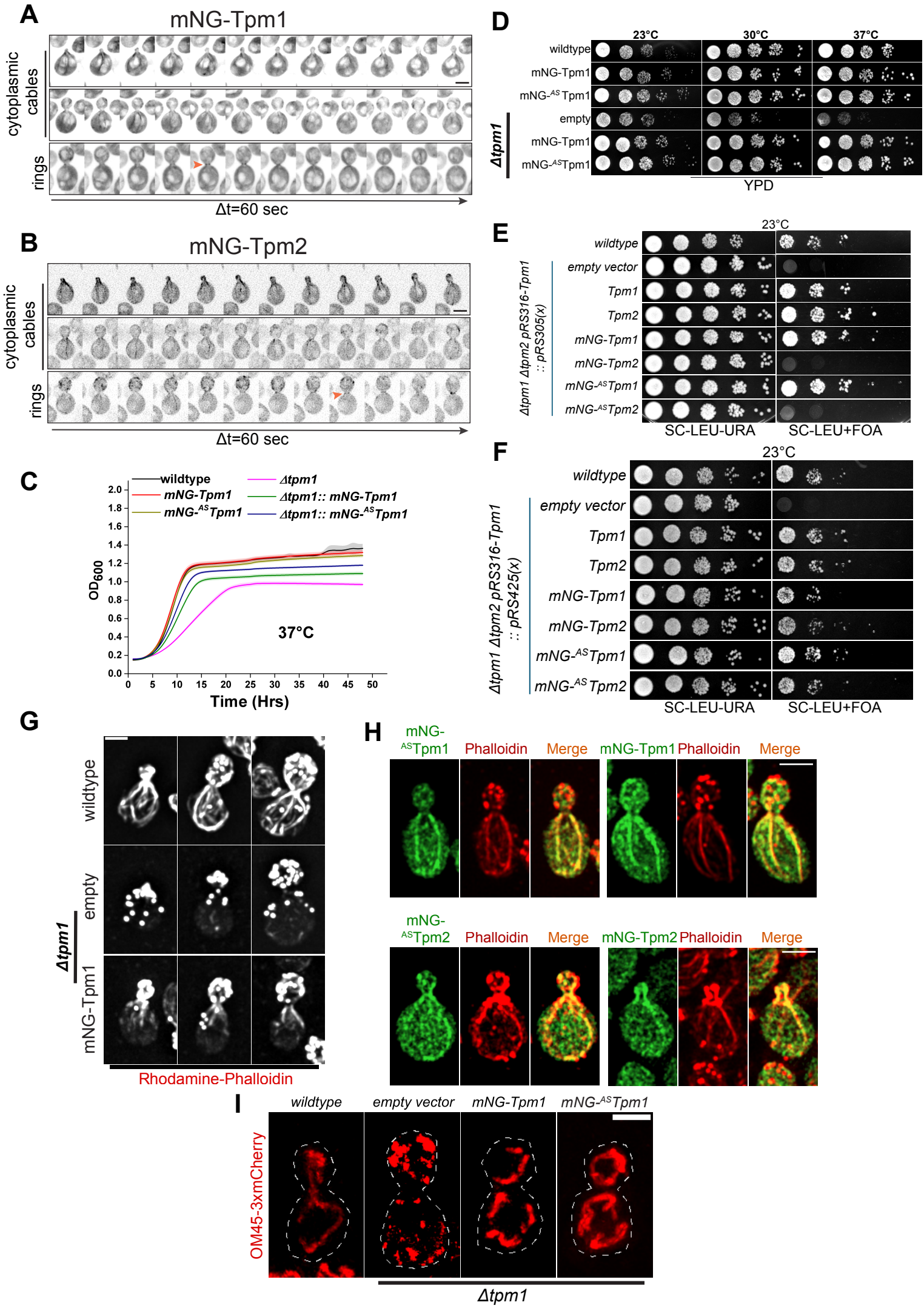
A
mNG-Tpm1
cytoplasmic cables
rings
Δt=60 sec
B
mNG-Tpm2
cytoplasmic cables
rings
Δt=60 sec
C
wildtype
mNG-Tpm1
mNG-ASTpm1
Δtpm1
Δtpm1:: mNG-Tpm1
Δtpm1:: mNG-ASTpm1
OD600
37°C
Time (Hrs)
D
23°C
30°C
37°C
wildtype
mNG-Tpm1
mNG-ASTpm1
empty
mNG-Tpm1
mNG-ASTpm1
Δtpm1
YPD
E
23°C
wildtype
empty vector
Tpm1
Tpm2
mNG-Tpm1
mNG-Tpm2
mNG-ASTpm1
mNG-ASTpm2
Δtpm1 Δtpm2 pRS316-Tpm1 :: pRS305(x)
SC-LEU-URA
SC-LEU+FOA
F
23°C
wildtype
empty vector
Tpm1
Tpm2
mNG-Tpm1
mNG-Tpm2
mNG-ASTpm1
mNG-ASTpm2
Δtpm1 Δtpm2 pRS316-Tpm1 :: pRS425(x)
SC-LEU-URA
SC-LEU+FOA
G
wildtype
empty
mNG-Tpm1
Δtpm1
Rhodamine-Phalloidin
H
mNG-ASTpm1
Phalloidin
Merge
mNG-Tpm1
Phalloidin
Merge
mNG-ASTpm2
Phalloidin
Merge
mNG-Tpm2
Phalloidin
Merge
I
wildtype
empty vector
mNG-Tpm1
mNG-ASTpm1
OM45-3xmCherry
Δtpm1

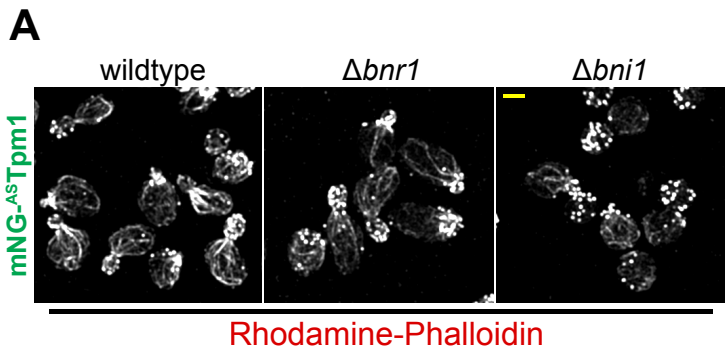
A
wildtype
Δbnr1
Δbni1
mNG-ASTpm1
Rhodamine-Phalloidin

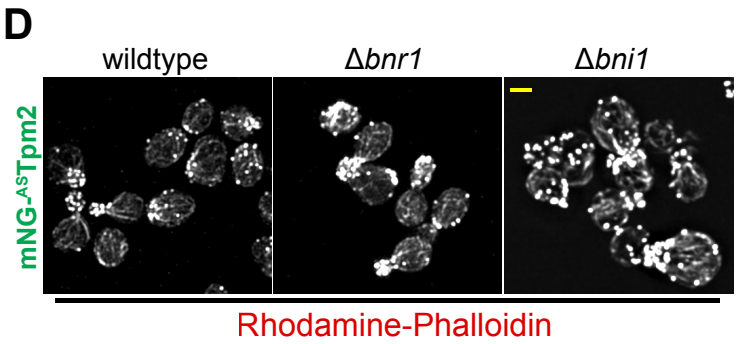
D
wildtype
Δbnr1
Δbni1
mNG-ASTpm2
Rhodamine-Phalloidin

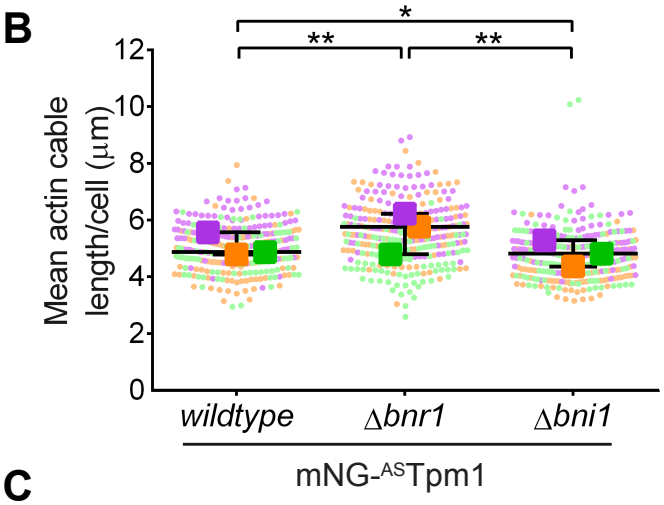
B
Mean actin cable length/cell (μm)
0
2
4
6
8
10
12
*
**
**
wildtype
Δbnr1
Δbni1
mNG-ASTpm1

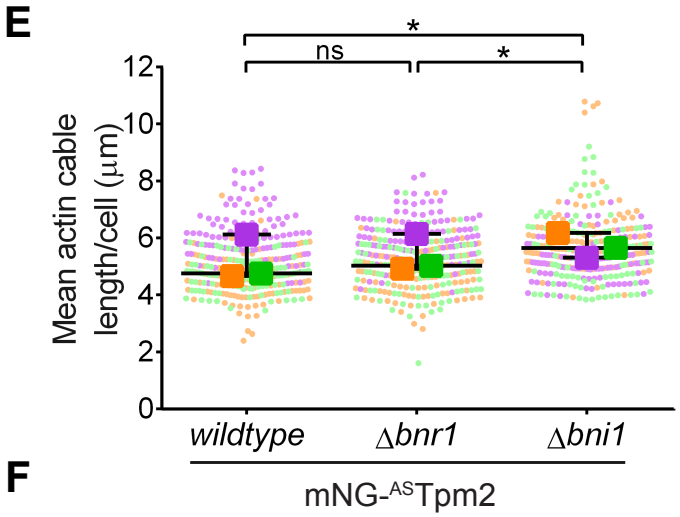
E
Mean actin cable length/cell (μm)
0
2
4
6
8
10
12
*
ns
*
wildtype
Δbnr1
Δbni1
mNG-ASTpm2

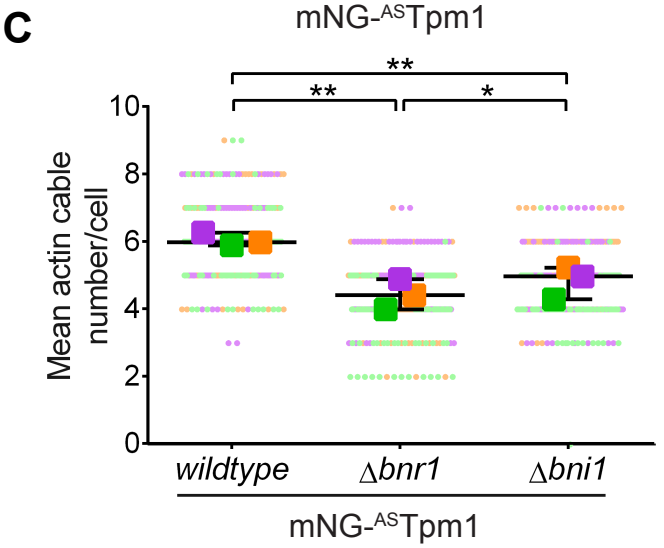
C
Mean actin cable number/cell
0
2
4
6
8
10
**
**
*
wildtype
Δbnr1
Δbni1
mNG-ASTpm1

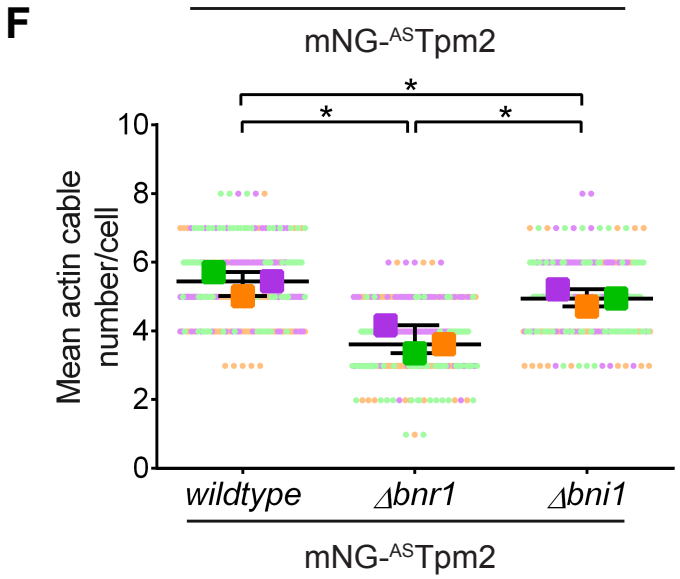
F
Mean actin cable number/cell
0
2
4
6
8
10
*
*
*
wildtype
Δbnr1
Δbni1
mNG-ASTpm2

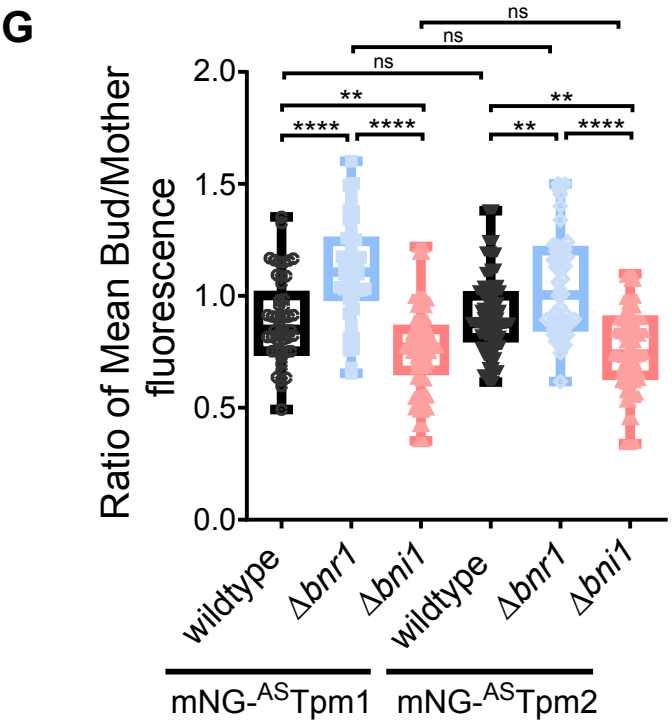
G
Ratio of Mean Bud/Mother fluorescence
0.0
0.5
1.0
1.5
2.0
ns
ns
ns
**
****
****
**
**
****
wildtype
Δbnr1
Δbni1
wildtype
Δbnr1
Δbni1
mNG-ASTpm1
mNG-ASTpm2

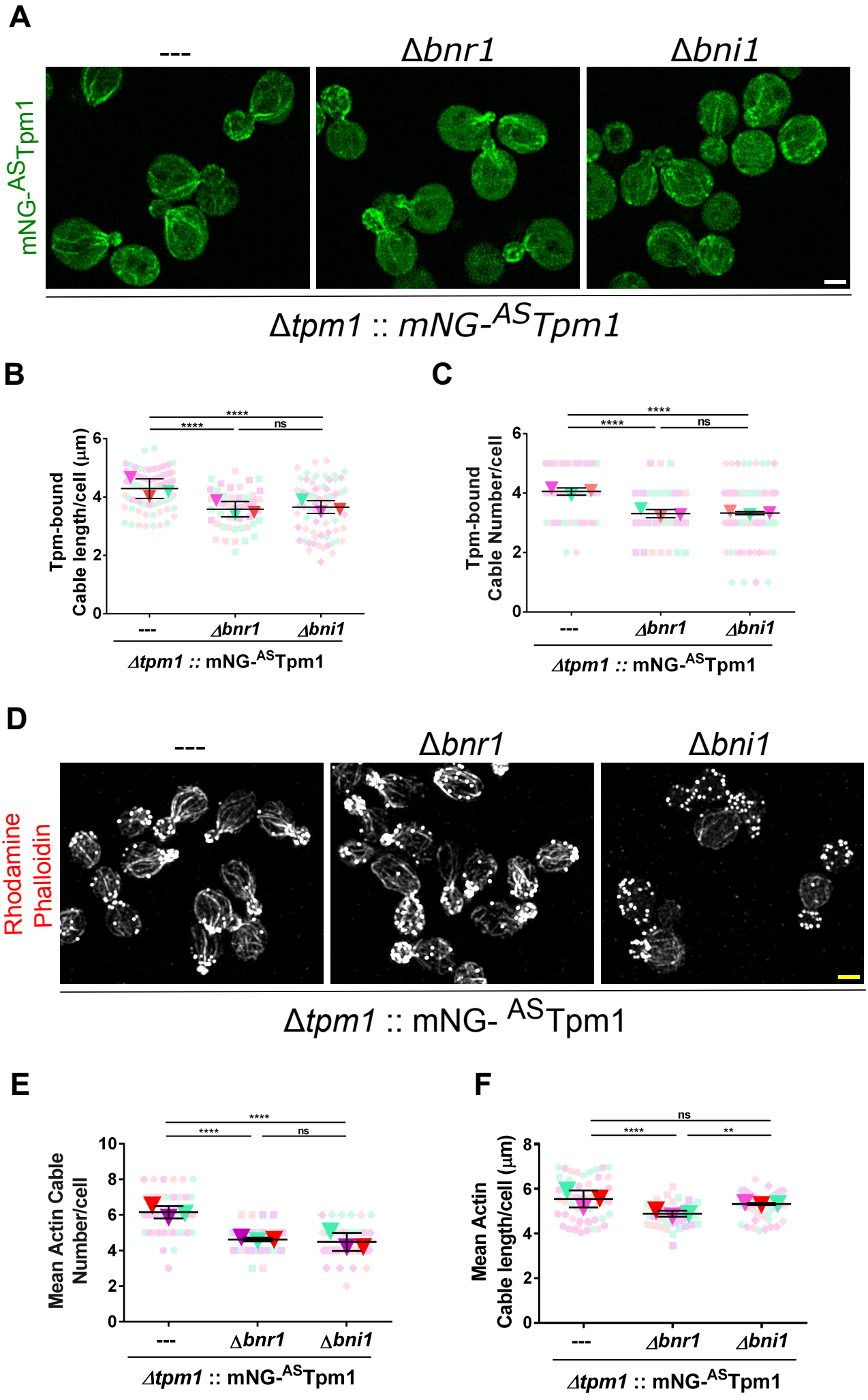
A

Δbnr1
Δbni1
mNG-ASTpm1
Δtpm1 :: mNG-ASTpm1
B
Tpm-bound Cable length/cell (μm)
****
****
ns

Δbnr1
Δbni1
Δtpm1 :: mNG-ASTpm1
C
Tpm-bound Cable Number/cell
****
****
ns

Δbnr1
Δbni1
Δtpm1 :: mNG-ASTpm1
D

Δbnr1
Δbni1
Rhodamine Phalloidin
Δtpm1 :: mNG- ASTpm1
E
Mean Actin Cable Number/cell
****
****
ns

Δbnr1
Δbni1
Δtpm1 :: mNG-ASTpm1
F
Mean Actin Cable length/cell (μm)
ns
****
**

Δbnr1
Δbni1
Δtpm1 :: mNG-ASTpm1

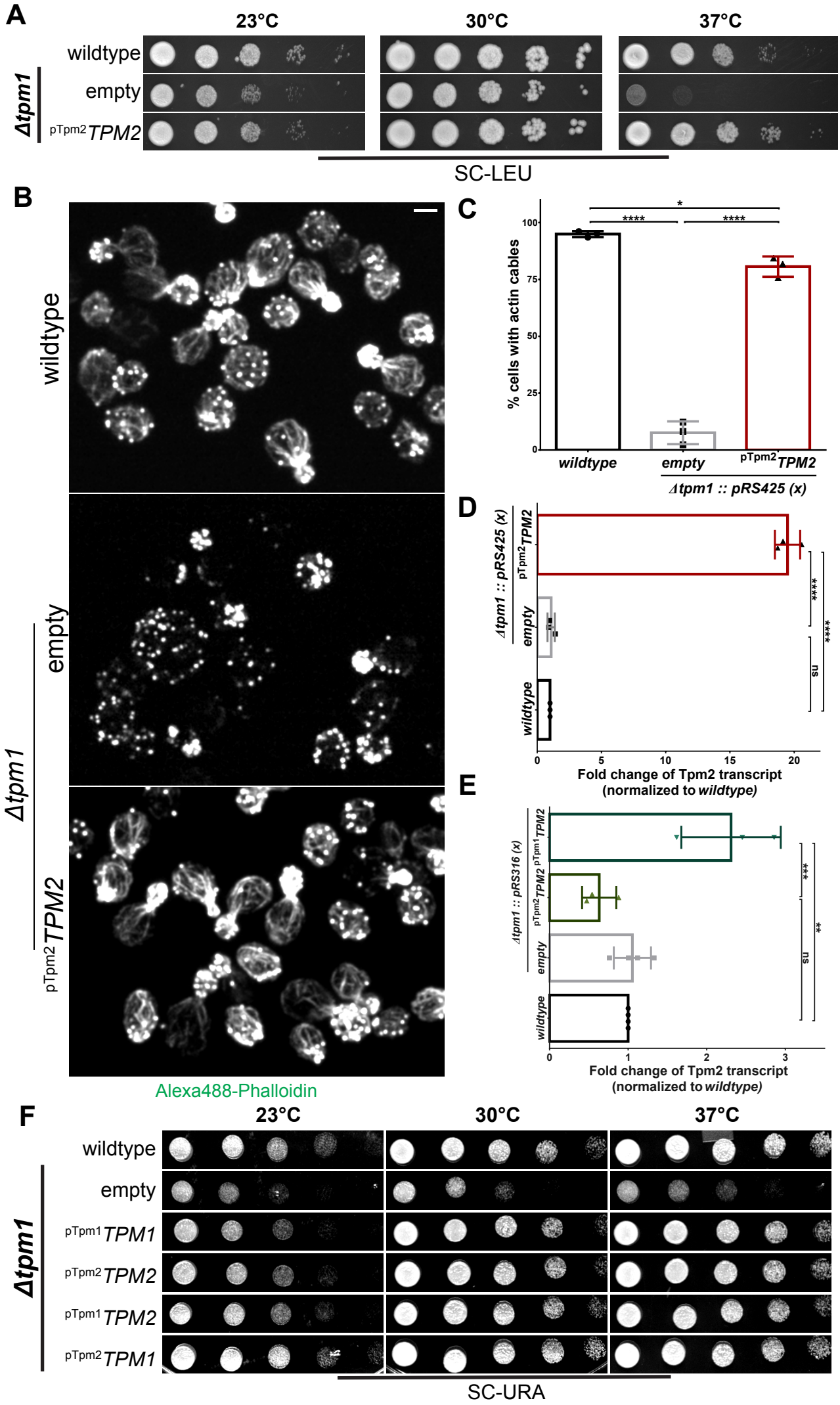
A
23°C
30°C
37°C
wildtype
empty
pTpm2 TPM2
Δtpm1
SC-LEU
B
wildtype
empty
pTpm2 TPM2
Δtpm1
Alexa488-Phalloidin
C
% cells with actin cables
100
75
50
25
0
*
****
****
wildtype
empty
pTpm2 TPM2
Δtpm1 :: pRS425 (x)
D
Δtpm1 :: pRS425 (x)
pTpm2 TPM2
empty
wildtype
****
ns
****
0
5
10
15
20
Fold change of Tpm2 transcript
(normalized to wildtype)
E
Δtpm1 :: pRS316 (x)
pTpm1 TPM2
pTpm2 TPM2
empty
wildtype
***
ns
**
0
1
2
3
Fold change of Tpm2 transcript
(normalized to wildtype)
F
23°C
30°C
37°C
wildtype
empty
pTpm1 TPM1
pTpm2 TPM2
pTpm1 TPM2
pTpm2 TPM1
Δtpm1
SC-URA

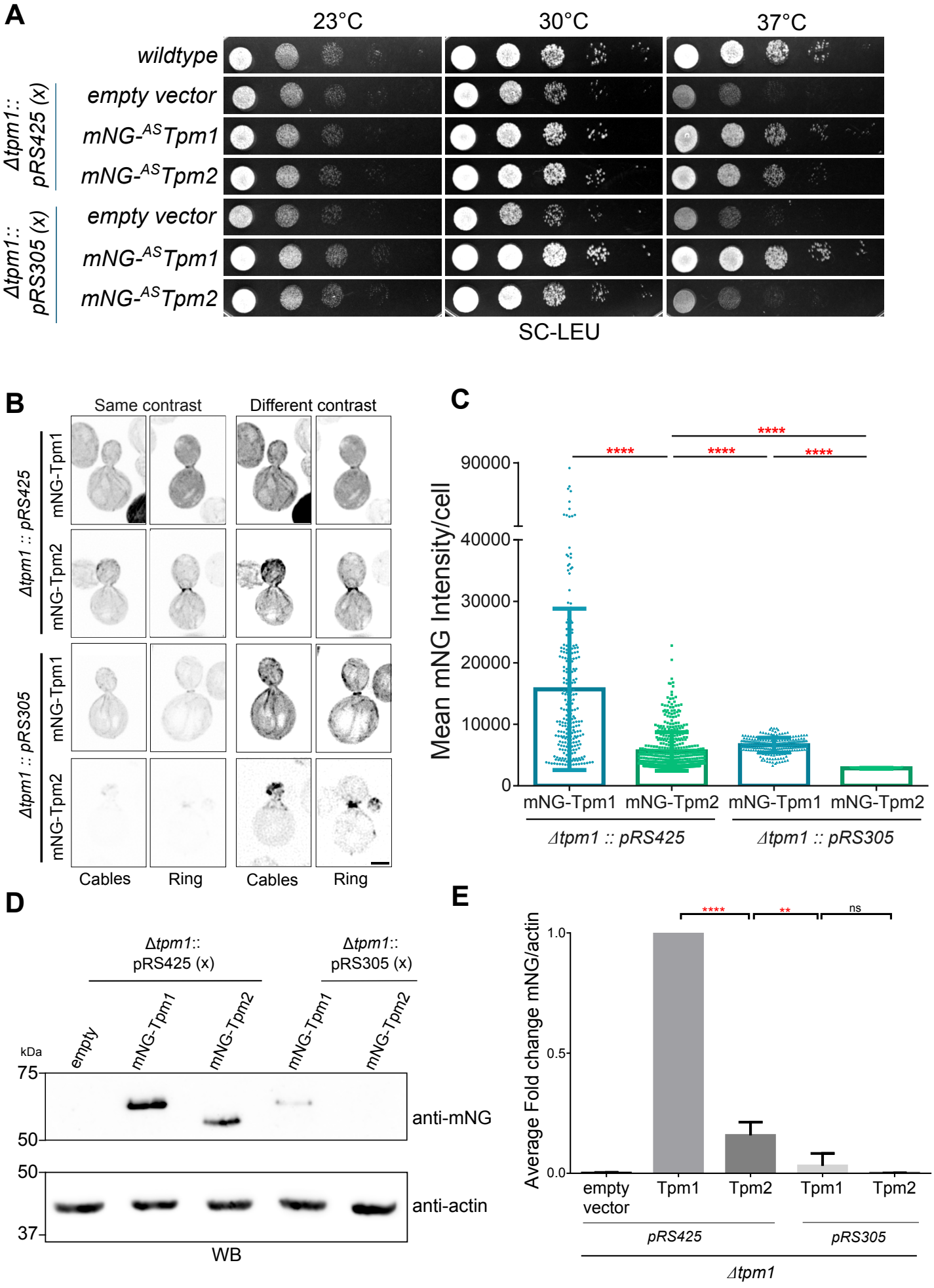
A
23°C
30°C
37°C
wildtype
empty vector
mNG-ASTpm1
mNG-ASTpm2
empty vector
mNG-ASTpm1
mNG-ASTpm2
Δtpm1:: pRS425 (x)
Δtpm1:: pRS305 (x)
SC-LEU
B
Same contrast
Different contrast
Δtpm1 :: pRS425
Δtpm1 :: pRS305
mNG-Tpm1
mNG-Tpm2
Cables
Ring
C
Mean mNG Intensity/cell
90000
40000
30000
20000
10000
0
****
mNG-Tpm1
mNG-Tpm2
Δtpm1 :: pRS425
Δtpm1 :: pRS305
D
Δtpm1:: pRS425 (x)
Δtpm1:: pRS305 (x)
empty
mNG-Tpm1
mNG-Tpm2
kDa
75
50
anti-mNG
anti-actin
37
WB
E
Average Fold change mNG/actin
1.0
0.5
0.0
****
**
ns
empty vector
Tpm1
Tpm2
pRS425
pRS305
Δtpm1

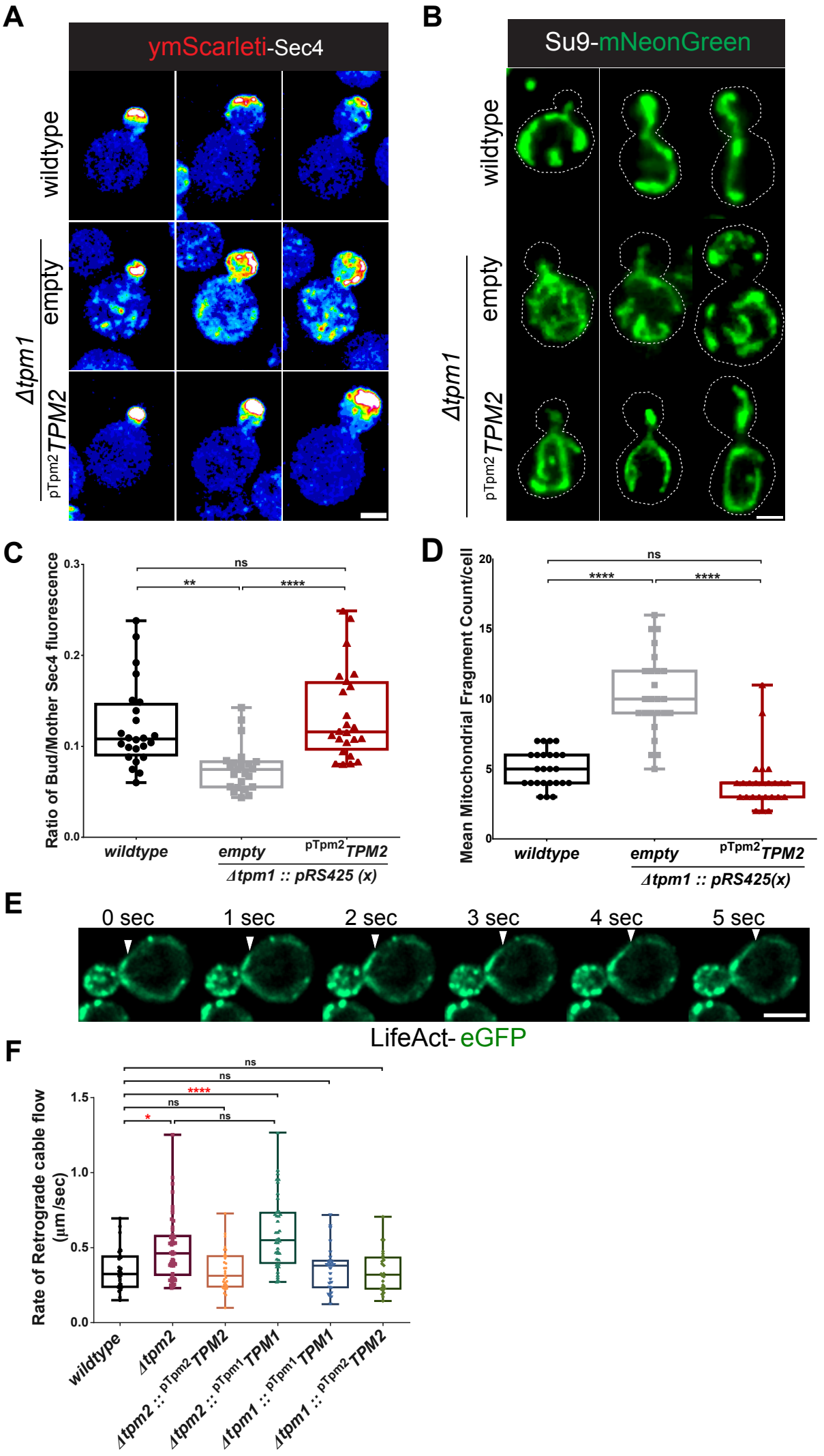
A
ymScarleti-Sec4
wildtype
Δtpm1
empty
pTpm2 TPM2
B
Su9-mNeonGreen
wildtype
Δtpm1
empty
pTpm2 TPM2
C
Ratio of Bud/Mother Sec4 fluorescence
0.3
0.2
0.1
0.0
ns
**
****
wildtype
empty
pTpm2 TPM2
Δtpm1 :: pRS425 (x)
D
Mean Mitochondrial Fragment Count/cell
20
15
10
5
0
ns
****
****
wildtype
empty
pTpm2 TPM2
Δtpm1 :: pRS425(x)
E
0 sec
1 sec
2 sec
3 sec
4 sec
5 sec
LifeAct- eGFP
F
Rate of Retrograde cable flow (µm/sec)
1.5
1.0
0.5
0.0
ns
ns
****
ns
*
ns
wildtype
Δtpm2
Δtpm2 :: pTpm2 TPM2
Δtpm2 :: pTpm1 TPM1
Δtpm1 :: pTpm1 TPM1
Δtpm1 :: pTpm2 TPM2

A

Actin Cable quantification Workflow (adapted from *McInally et al., 2022 (bio-protocol)*)

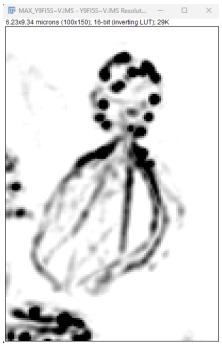

Inverted Grayscale image

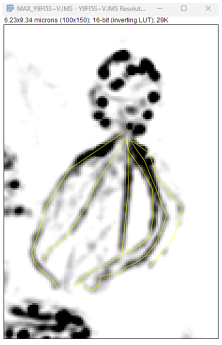

Traced actin cables in Fiji

Run script in Anaconda:

actin_cable_length_analysis.py

Adapted from McInally et al., 2022

B

Mitochondrial Fragement Number quantification

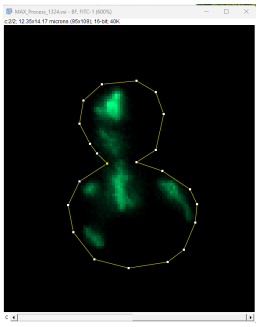

Mitochondrial signal

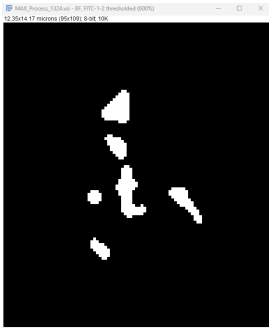

Segmented mitochondrial network using Mitochondria Analyzer Plugin

Measure mitochondrial fragment number in Fiji using "Analyze Particles"
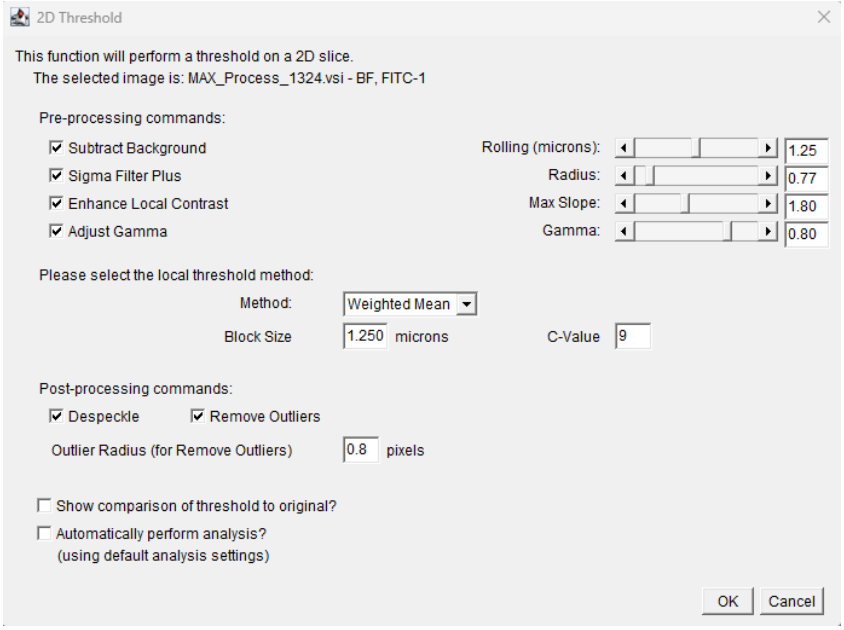
2D-Threshold paramters used in Mitochondria Analyzer Plug-in